2013

Inverse Problems In Multiple Light Scattering

John Broky
University of Central Florida

INVERSE PROBLEMS IN MULTIPLE LIGHT SCATTERING

by

JOHN BROKY
B.S. University of Arizona, 2004
M.S. University of Central Florida, 2007

A dissertation submitted in partial fulfillment of the requirements
for the degree of Doctor of Philosophy
in the College of Optics and Photonics
at the University of Central Florida
Orlando, Florida

Spring Term
2013

Major Professor: Aristide Dogariu

ABSTRACT

The interaction between coherent waves and material systems with complex optical properties is a complicated, deterministic process. Light that scatters from such media gives rise to random fields with intricate properties. It is common perception that the randomness of these complex fields is undesired and therefore is to be removed, usually through a process of ensemble averaging. However, random fields emerging from light matter interaction contain information about the properties of the medium and a thorough analysis of the scattered light allows solving specific inverse problems. Traditional attempts to solve these kinds of inverse problems tend to rely on statistical average quantities and ignore the deterministic interaction between the optical field and the scattering structure. Thus, because ensemble averaging inherently destroys specific characteristics of random processes, one can only recover limited information about the medium.

This dissertation discusses practical means that go beyond ensemble averaging to probe complex media and extract additional information about a random scattering system. The dissertation discusses cases in which media with similar average properties can be differentiated by detailed examination of fluctuations between different realizations of the random process of multiple scattering. As a different approach to this type of inverse problems, the dissertation also includes a description of how higher-order field and polarization correlations can be used to extract features of random media and complex systems from one single realization of the light-

matter interaction. Examples include (i) determining the level of multiple scattering, (ii) identifying non-stationarities in random fields, and (iii) extracting underlying correlation lengths of random electromagnetic fields that result from basic interferences. The new approaches introduced and the demonstrations described in this dissertation represent practical means to extract important material properties or to discriminate between media with similar characteristics even in situations when experimental constraints limit the number of realizations of the complex light-matter interaction.

To my wife, Deb

ACKNOWLEDGMENTS

It is difficult to express how gracious I am for all the guidance and kindness I've received from those I've met during my time at CREOL and the University of Central Florida. I'd first like to thank my advisor, Dr. Aristide Dogariu for the countless hours of mentoring and the feedback he's given me. He's always pushed me to expand my knowledge to all realms of optical topics and challenged me with wide range of research areas and projects and never let me put forth anything but my best work.

I also appreciate the participation and constructive comments that my committee as have given towards my research and dissertation work. I'd especially like to thank Dr. Demetrios Christodoulides for always making me feel welcome when collaborating with him and his students on additional research work.

I must also thank the entire Photonics Diagnostics of Random Media Group because I certainly didn't do this alone. They have always provided a pleasant working environment and given me friendship throughout my entire PhD career. I would specifically like to thank Dr. Jeremy Ellis for initially taking me under his wing teaching me the ropes of polarization and coherence. I'd like to thank Dr. Chaim Schwartz for being a great office mate and stepping in countless times to assist me during my first year of studies. I must also acknowledge Dr. David Haefner who joined the group at the same time, showing me the ropes of MATLAB and also inspiring me to always work harder. He also continued to encourage me and assist me in always improving my personal health and strength. I must also thank Dr. Thomas Kohlgraf-Owens for

providing countless hours of company sharing an office together and for Dr. Sergey Sukhov for just being a great friend. I've been a member of the group for a number of years and have made friends with a number of members both past and present, and though the list is long I must name them all: Janghwan Bae, Dr. Erwan Baleine, Dr. Gabriel Biener, Colin Constant, Lorrene Denney, Kyle Douglass, Veerachart Kajorndejnukul, Dana Kohlgraf-Owens, Kortan Ogutman, and Dr. Mohamed Salem. I must also mention that I've also been surrounded by brilliant minds here at CREOL and supportive peers, especially Chuck Williams and Mark Ramme.

I'd like to thank my friends and family for all the love they've given me before all my studies even began. I never would have achieved anything without your support. Thank you Mom, Dad, Beck, Rachel, Grandma and everyone else who's known me over all these years.

Finally, I give all my appreciation and thanks to my beautiful and most amazing wife, Deborah. She's basically been with me every step of the way supporting me, always by my side, and always ready to help in any way she can. She inspires me to be better, keep striving for more, and encouraging me and reassuring me that I can achieve anything. I love you so much. And I'll close with some very important words of wisdom she's given me that I always keep close to me. "Hang in there, keep focused, work hard – you can do it!"

TABLE OF CONTENTS

LIST OF FIGURES

CHAPTER 1: INTRODUCTION

A common way to describe the wave interaction with disordered media is through Boltzmann theory for incoherent transport, which implicitly includes an average over all possible realizations of disorder and neglects possible interference effects [1]. The outcome is characterized statistically through expectation values for different parameters describing the interaction. However, in mesoscopic systems when the characteristic scale of interaction is less than the phase coherence length, this simplified description is insufficient.

Because of the generality of the problem and its implications in many different fields, the interaction between coherent waves and random media in the mesoscopic regime has been intensely studied. Electromagnetic (EM) waves and light in particular, constitute a convenient tool to examine the physics of random media and test theoretical concepts. For instance, light scattering experiments can be conducted in geometries not accessible in electronic conductance studies. In this context, research on the statistical properties of scattered intensities has been particularly interesting because of the discovery of enhanced fluctuations [2] in transmission and in electronic conductance [3].

A random medium is usually characterized by an ensemble of realizations of disorder. When waves interact with a random medium, each member of this ensemble, i.e. each particular realization of disorder, has its own specific pattern of fluctuations in the scattered wave. The complicated features of the scattered waves are all rooted in the structural properties of a specific realization of randomness. One could therefore argue that, in principle, the inverse problem can be solved if (i) the phase coherence is maintained over the entire interaction, (ii) the process is

not dissipative, and (iii) the disorder does not vary in time. However, due to experimental limitations one always infringes at least on the second requirement. Furthermore, the information available is often too complex to process in a practical manner. This is why the average over an ensemble of structural realizations is usually taken to determine mean statistical properties. For instance, when coherent light interacts with a random medium, the scattered intensity fluctuations resulting from different realizations of the interaction must be averaged to learn about the global material properties [4,5]. One must realize though that this averaging inherently discards information specific to a particular realization or regarding variations from one realization to the next.

A couple of questions arise when only considering an ensemble of the complex wave-matter interaction. Is it possible to learn more about the medium by closely examining the emerging fluctuations? Is it possible to determine the stochastic properties without requiring an ensemble of realizations? To go beyond the information embedded in ensemble averages, it is important to grasp some of the basic properties of random electromagnetic fields and their intensity fluctuations. Chapter 2 of this dissertation reviews many of the commonly known properties of intensity fluctuations that may result from a number of light scattering situations. In addition to understanding how the intensity behaves, which represents the scalar approach to describing the problem, it is sometimes even more important to understand the vectorial fluctuations that occur and thus to examine the polarization of the random electromagnetic fields.

There are a number of techniques that attempt to solve inverse scattering problems in the regime of multiple scattering. A few traditional approaches are discussed in Chapter 3. As mentioned above, a number of these procedures depend on ensemble measurements to calculate statistical average values of the scattering medium. But, is it possible to have to structurally

different media which have identical average properties and is it possible to differentiate between them? The statistics of fluctuations that result from the scattering of light provide the means. Whether the fluctuations are in intensity, phase, or polarization, they all result from the light interaction or, in other words, from the ``sampling" of the medium. These fluctuations relate to the medium's stochastic properties.

Many practical situations are such that an ensemble of realizations of the random medium is not available or it is too prohibitive in time or measurement resources. Chapter 4 discusses means to take advantage of the sampling of the light interaction in a single realization of the light-matter interaction. A key factor to examine is that the intensity is not the only fluctuating property that can be conveniently used to learn about the properties of the medium; observing fluctuations in the polarization of light is also useful. Importantly, fluctuations of polarization can exist on different length scales than intensity variations and this observation offers unique possibilities. For instance, the fluctuations of polarization in a single realization of light-matter interaction can reveal field non-stationarities that otherwise could be observed only upon ensemble average. Fluctuation in the polarization properties of scattered fields can also be used to differentiate between scattering media and to extract underlying correlation lengths of individual scatterers.

Although random fluctuations in electromagnetic fields are often considered as undesired noise needing to be suppressed and removed, the fields contain a wealth of information. This dissertation seeks to demonstrate that not only can the fluctuations in optical fields be used to solve inverse problems to learn about scattering media but much of this can be done without access to an ensemble but instead from a single realization of light-matter interaction.

CHAPTER 2: STATISTICAL FLUCTUATIONS IN SCATTERED LIGHT

As mentioned in the previous chapter, one can learn quite a bit about a complex scattering medium by analyzing the light scattered by it. In order to maximize the ability to extract information from scattered light, it is important to understand the nature of the light-matter interaction. Since the optical fields pick up random phases through propagation and surface scattering, the measured properties manifest themselves as fluctuations in field amplitude and intensity. In this chapter we will discuss the general statistics of the fluctuations that occur in scattered light, specifically the intensity as this is the primary measurable in optical regimes.

2.1 Scalar Statistics of Intensity Fluctuations

A very common instance of intensity fluctuations occurs spatially and occurs on reflection. When a coherent continuous-wave light source is incident upon a surface, the reflected, scattered light is seen as a high contrast "grainy" pattern known as speckle. The speckles are caused from the interference of scattered waves that acquired random phases [4,6]. In reflection, or backscatter, this may be caused from the presence of a rough surface or volume media where the light bounces in all directions and travels different paths. This can also be observed in transmission, such as through a diffuse material or a particle suspension, where the optical paths of photons differ significantly in length on the order of a wavelength. A simple description of how speckles are caused is by describing the process as a random walk in the phase space, where a large number of complex components are added together, having random lengths and random directions [7,8]. The resultant sums may be either large or small depending on whether constructive or destructive interference dominates. The squared length of the

resultant phasor is equivalent to the intensity and thus appears as the bright and dark spots known as speckles.

Speckles constitute a random process and its properties are described statistically. The most basic defining nature of a speckle pattern is the probability distribution of its intensity values. For a fully developed speckle, in which the phases are uniformly distributed, the probability distribution of intensity follows a negative exponential $p(I) = (1/\bar{I})\exp(-I/\bar{I})$.

Another common descriptor of speckle is the contrast C, the ratio of the standard deviation of intensity σ_I to its average intensity $\bar{I}$, $C = \sigma_I / \bar{I}$. The contrast is a simple measure of the strength of the intensity fluctuations. For a fully developed speckle field the contrast is equal to one. The contrast decreases for cases when the speckle is not fully developed. This can occur in cases where a large number of random contributions are added to a known or constant contribution such as in holography where there is a known reference, or when the roughness of the object is smaller than the wavelength [7].

Contrast also decreases when adding two uncorrelated speckle patterns. This is an addition in intensity and can occur from illuminating the medium with different angles of incidence, orthogonal polarizations, or multiple wavelengths [9]. In general, when adding N independent random fields the minimum contrast (resulting from equivalent average intensities) decreases as $C = 1/\sqrt{N}$.

Besides the distribution of intensity fluctuations, there are a number of correlations that can occur between the interference of two diffuse intensities. The most common correlations are referred to as short range, long range, and "infinite" correlations, denoted by C_1, C_2, and C_3 respectively [2,5,10].

A simple way to realize the meaning of these correlations is to think of the scattering media as a multi-channeled interface, where light can enter any of the input channels and then exit through a corresponding exit channel. When considering a single channel, where light enters at a and then exits at b, one can define the angular transmission coefficient, T_{ab}. The angular transmission is associated with the C_1 correlation function, otherwise known as short range correlations [2,11]. It describes the intensity fluctuations between the dark and bright transmission intensities.

As the C_1 correlation is the correlation of speckles near to each other, it is also primarily associated with the geometric size of the speckle. A speckle pattern consists of a large number of peaks and valleys, so any scale associated with the speckle size would need to be an average. On the outgoing surface of the media (the exiting channels) the speckle size is on the order of the wavelength λ, and then expands as it propagates to the observation plane [6]. A simple experimental way of measuring the average size of a speckle is to perform an autocorrelation. This is a simple C_1 correlation of a speckle with itself. For fully developed speckle patterns, the size is defined as $\delta x = z\lambda / D$ where, λ is the wavelength of light, z is the propagation distance from medium to observation plane, and D is the diameter of the illumination spot [7]. It has also been shown that there is memory of the initial angle of illumination [2,12]. Over a small angular range, as the angle of illumination changes, the speckle pattern will shift, and eventually decorrelate.

In addition to the speckle size and angular correlation, there are a number of higher order correlations associated with speckles, or more generally intensity fluctuations that vary over a number of different scales. The first of these is the C_2 correlation, or long-range correlation,

which is associated with the total transmission [13]. These correlations are very weak and for a single channel in, single channel out configuration, are only seen in very strongly scattering media that are close to Anderson localization [14]. This type of correlation is much more easily measured when all outgoing channels resulting from a single incoming channel are added up, an operation typically performed with an integrating sphere [15]. The total transmission T_a resulting from channel a is a result of integrating over all outgoing channels, $T_a = \sum_b T_{ab}$. The C_2 contribution is the correlation of two speckles that are far apart and in which the C_1 contribution is completely overwhelmed [16].

The third correlation type is C_3 and is seen experimentally as considering all channels going in and all channels coming out, $T = \sum_a T_a = \sum_{ab} T_{ab}$. It is often called the conductance as an analogy to electronic systems, or as the "infinite"-range correlation as it has contributions from all incoming and outgoing angles [3,17]. In electronics, the fluctuations of C_3 are often called the universal conductance fluctuations (UCF) but these are very difficult to observe in optics [18]. These fluctuations are static and not temporal as the scatterers in the medium are fixed, and the variance of the fluctuations is independent of common material parameters such as sample thickness, and mean free path [19].

2.2 Suppressing Intensity Fluctuations

The most obvious way to address fluctuations in intensity is actually to try to remove them. Speckles caused from coherent illumination are often unwanted and are removed through ensemble averaging, or broadband sources. When illuminating rough objects with coherent light, such as a laser, it is expected that the image will be marred with speckles. This reduces the

ability to resolve details of the object and can sometimes lead to a completely indistinguishable image. In principle, to “remove” speckles, the goal is to reduce the overall speckle contrast.

A simple way to reduce the speckle contrast is through the use of polarization diversity. As will be addressed in more detail in the next section, partially polarized speckle has a reduced contrast. When the scattered light has contributions in two orthogonal polarizations, the two speckle patterns in those polarizations are independent of each other [7]. Adding these two independent speckles together in intensity reduces the contrast. The same can be said for illuminating the object with different polarization states. Illuminating with different polarization states also leads to two independent speckle patterns in the orthogonal polarization states [20]. Figure 2-1a shows a simple schematic of inserting both a polarizer on input and polarization analyzer to create independent speckle patterns. When the incident polarization state, and polarization analyzer switch states faster than the integration time of the detector, the resulting signal is essentially an ensemble of four independent speckle patterns, potentially reducing the contrast by half [7].

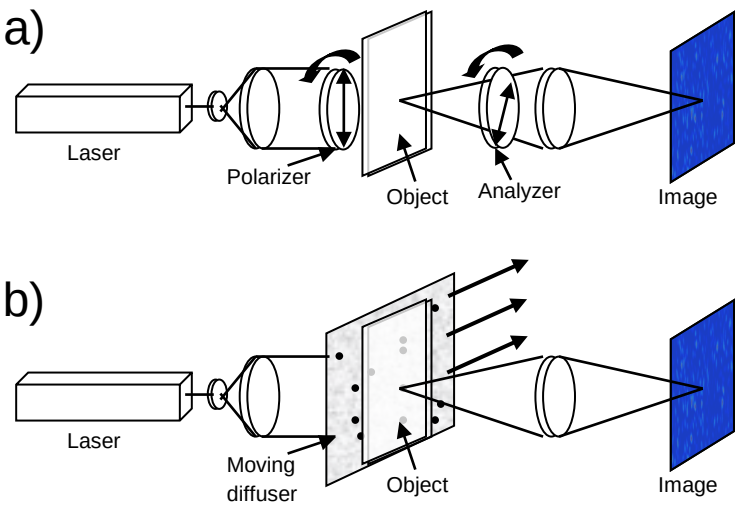

Figure 2-1: Speckle suppression techniques. (a) Using rotating polarizers on both input and output. (b) Moving a diffuser in front of object.

Another potential method is to change the dynamics of the source, such as using a moving diffuser close to the object, Figure 2-1b. The diffuser itself creates random interference and a speckle pattern of its own. The object is essentially illuminated with a speckle pattern and as the diffuser moves, the illuminating speckle pattern in turn changes. This causes each point on the object to experience a changing phase and with each new realization of the random walk through the object, the intensity of the speckles in the scattered field change. Again, with a large enough ensemble of the resulting scattered field, the integration over a number of independent speckle realizations reduces the contrast. With the right speed of the diffuser and integration of the detector, the contrast of the speckles reduces, leaving the wanted signal of the object to rise above the averaged background.

There has been other work to remove speckles in the far field using similar principles such as employing diffractive optic elements [21] or a stationary multimode fiber [22] in projection systems typically plagued with speckle. There has also been recent developments in

random lasers capable of a very low spatial coherence [23]. By tuning the random laser to have a very low spatial coherence, it breaks down the strong interference of the laser source from the medium and they can achieve nearly speckle-free imaging [24].

2.3 Polarization in Scattered Fields

Beyond the scalar properties discussed in the previous section, it is important to consider the vectorial properties. The most accessible aspect of vector statistics is to consider the polarization. The polarization properties of speckle are very unique and are another factor that contributes to the scalar intensity contrast. Light scattered from an incident polarized beam has unique polarization properties that depend on the scattering medium. The light scattered from a rough dielectric surface such as paper, is a multiple scattering process and produces an overall field that is unpolarized. In general, since a speckle is the result of an interference effect, each individual speckle will be fully polarized but may have its own unique state [7]. Thus, in a strong multiple scattering case, the speckle pattern is said to be globally unpolarized; all speckles have random, yet pure polarization states that collectively represent some or all possible polarizations states. Another way to observe globally unpolarized speckle is to view the pattern through an analyzer oriented along the $\hat{x}$ or $\hat{y}$ directions. The resulting speckle patterns observed are uncorrelated and will look nothing alike.

For the case of scattered light off of a rough metal surface, the resulting scattered light is considered globally polarized, in which each speckle component of the scattered field shares the same state. Unlike the above example, scattering from a rough metallic surface is dominated by strong single scattering in which the initial polarization state is maintained. In this case,

observing the pattern through orthogonal polarization analyzers would show two similar patterns that are well correlated.

The resulting contrast of these polarized and unpolarized speckles is highly dependent on the global degree of polarization $\bar{P}$ of the entire scattered field,

$$\bar{P} = \frac{\sqrt{\int_A S_1^2 dr + \int_A S_2^2 dr + \int_A S_3^2 dr}}{\int_A I dr}, \tag{2.1}$$

where

$$S_1(r) = E_x^*(r)E_x(r) - E_y^*(r)E_y(r), \tag{2.2}$$

$$S_2(r) = E_x^*(r)E_x(r) - E_y^*(r)E_x(r), \tag{2.3}$$

$$S_3(r) = i\left(E_x^*(r)E_y(r) - E_y^*(r)E_x(r)\right), \tag{2.4}$$

As the degree of polarization decreases, so does the contrast following the relation

$$C = \sqrt{\frac{1+\bar{P}^2}{2}}. \tag{2.5}$$

The loss in contrast is due to a global quantity. A low degree of polarization is due to a large collection of randomly polarized speckles in the scattered field, but there is still some memory of the incident polarization state. A set of universal polarization correlations developed by Freund, et al. show that there is indeed strong correlation of the scattered field and the incident polarization state [20].

The scattered field components are assigned $E_{in,out}$ such that E_{yx} represents a x-polarized output resulting from a y-polarized input. Using a notation where $xx = 1$, $xy = 2$, $yx = 3$, and $yy = 4$, the correlation matrix of the scattered fields simplifies to

$$C = \begin{pmatrix} 1 & 0 & 0 & \Gamma \\ 0 & \rho & \delta & 0 \\ 0 & \delta^* & \rho & 0 \\ \Gamma^* & 0 & 0 & 1 \end{pmatrix}, \tag{2.6}$$

where $C_{ij} = \langle E_i E_j^* \rangle$ and $\langle \ldots \rangle$ denotes an ensemble average [20]. There are three important material parameters that lie within this correlation matrix, the depolarization ρ, and Γ and δ, which describe the partial correlation of the scattered light. These parameters have a special relation in that $\Gamma + \delta = 1 - \rho$ and that as the scattering increases (strong multiple scattering) ρ approaches unity while Γ and δ reduce to zero. This can be seen from a simple model of a random arrangement of point scatterers [25,26]. Based upon this model, expressions relating to the number of scattering events n before exiting the scattering medium follow [27]

$$\Gamma_n = (3/2)(7^m + 5^m)/(10^m + 2 \cdot 7^m), \tag{2.7}$$

$$\delta_n = (3/2)(7^m - 5^m)/(10^m + 2 \cdot 7^m), \tag{2.8}$$

$$\rho_n = (10^m - 7^m)/(10^m + 2 \cdot 7^m), \tag{2.9}$$

where $m = n - 1$. Again, it's easy to see that when $n = 1$ (single scattering), both δ and ρ vanish, demonstrating that single scattering preserves the input polarization state. As can be seen in Figure 2-2, as n becomes very large, ρ approaches unity while Γ and δ vanish.

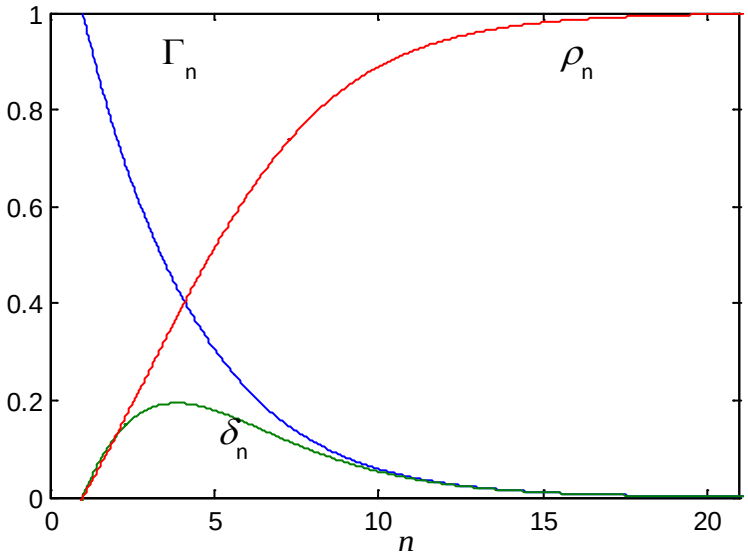

Figure 2-2: Material parameters Γ_n, δ_n, and ρ_n for point scatterers versus the number of scattering events n.

The correlation material parameters can be further expanded by relating them to the better known Stokes parameters

$$S_0 = S_0' = 1, \tag{2.10}$$

$$S_1 = \left[(1-\rho)/(1+\rho)S_1'\right], \tag{2.11}$$

$$S_2 = \pm\left[(\Gamma+\delta)/(1+\rho)S_2'\right], \tag{2.12}$$

$$S_3 = \pm\left[(\Gamma-\delta)/(1+\rho)S_3'\right], \tag{2.13}$$

where S' is the normalized Stokes input. This enables for ease of measurement within experiments. In fact, direct measurements of Γ and δ can prove to be difficult as they require appropriate speckle patterns to correlate. Thus, Γ and δ can be calculated by inverting Eqs.

(2.12) and (2.13) provided that elements of the incident Stokes vector are non-zero, i.e. non-linear.

From these correlations, a sort of parallel to the above example of observing a speckle pattern through orthogonal analyzers is the result of illuminating the media with orthogonal polarizations. A scattering medium can create partially polarized speckles that have polarization vectors in the orthogonal states. These occur as independent speckles when viewed through orthogonal analyzers. The same can occur when illuminating the same medium with orthogonal states. The correlation of the two speckle fields reduces as the input state rotates. The amount of decorrelation again depends on the strength of scattering of the medium and for a sample with arbitrary depolarization, the correlation follows

$$C(\theta,\theta_0) = (1-\beta)cos^2(\theta-\theta_0)+\beta, \tag{2.14}$$

where $\beta = (1-\rho)^2/(1+\rho^2)$ and θ_0 represents the initial orientation of incident polarization state and θ represents the rotation of the incident state. Examples of correlations for different scattering media are shown in Figure 2-3. A rough metallic surface (Figure 2-3b) still shows high correlation regardless of the input state as it has $\rho \approx 0$. This signifies a polarization memory in the scattered speckle field. “Knowledge” of the incident polarization state is maintained as it scatters through the medium, even a strongly scattering depolarizing medium. The Stokes vector of illumination with arbitrary polarization can also be recovered after scattering by correlating four appropriately chosen speckle fields [28,29].

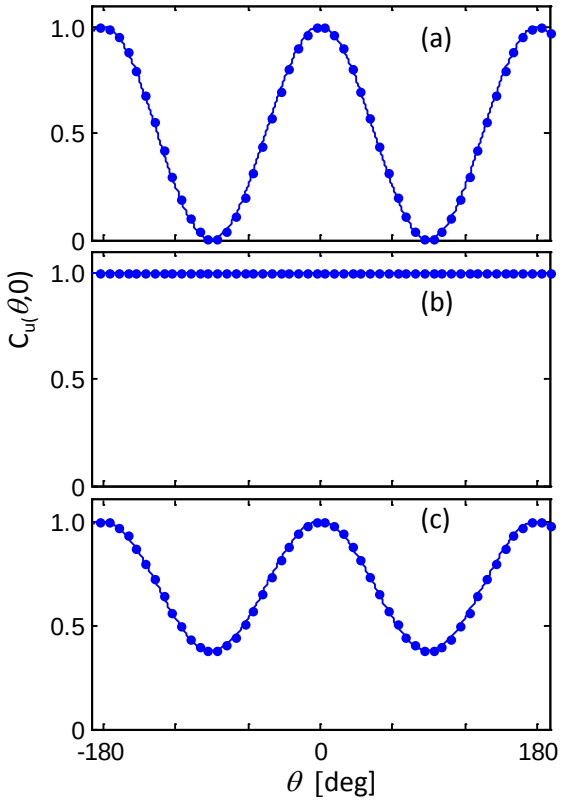

Figure 2-3: Correlation functions in reflection with no output polarizer for three different scattering media (a) $\rho = 0.95$, (b) $\rho = 0.005$, and (c) $\rho = 0.35$.

Beyond the correlation parameters and the depolarization of scattered optical waves, also of interest is the distribution of polarization states of multiply scattered fields. Since the polarization is a vector quantity, a simple measure of polarization is its ellipticity. From the intensity distribution functions $P_a(I_a)$ and $P_b(I_b)$ for the major and minor axes respectively, the distribution function for ellipticity can be found [30]. In the case of complete depolarization $\rho = 1$, a full complement of randomly polarized fields, the distribution function for ellipticity $\varepsilon = (I_b/I_a)^{1/2}$ is of the form [30,31]

$$P_{\varepsilon}(\varepsilon) = \frac{2(1-\varepsilon^2)}{(1+\varepsilon^2)^2}. \tag{2.15}$$

It's easy to see that it is at a maximum when $\varepsilon = 0$ and minimum when $\varepsilon = 1$, but perhaps must intriguing is that its expected value $\langle \varepsilon \rangle = 1 - ln2 = 0.307$. This shows that the most probable polarization in the randomly scattered field is mostly linear, with circular states mostly improbable [30].

2.4 Non-Gaussian Unpolarized Fields

As mentioned before, the polarization of scattered light resulting from a strongly scattering medium is said to be globally unpolarized ($\bar{P} = 0$). Since the speckles are a result of random coherent superpositions, each individual speckle is theoretically fully polarized, yet may be in a completely different state of polarization from its neighboring speckle. These polarization state fluctuations give rise to the global depolarization, an average quantity.

There have been several studies that have gone into the nature of the polarization states of speckles and how they relate to the media that created them [20,27,29,30]. The means stem from the nature of how to describe unpolarized fields. Essentially all experimentally measured polarization is a time averaged quantity. Instantaneously all waves are fully polarized, but may jump randomly from one state to another from one instant to the next. Since all detectors average the light received over a finite amount of time, the wave may appear unpolarized. The same can be applied spatially, where a polarization state is derived from the statistics of underlying random complex fields. An easy way to visualize a number of polarization states is on the observable polarization sphere [32]. It is possible that the underlying fields are locally unpolarized, and with this case only the intensity statistics are retrievable. It is also possible that

the underlying fields are locally pure states of polarization and the distributions of the states on the observable polarization sphere can reveal more about the wave-matter interaction.

There are a number of different distributions of polarization states that can lead to a globally unpolarized field. These distributions all stem from the simple case of one polarization state canceling another; such is the case with two orthogonal polarization states. A uniform distribution on the observable polarization sphere defines the first type of unpolarized light. Type I unpolarized light is invariant to rotation on the observable polarization sphere and is symmetric about a specific plane. A common cause of Type I is the combination of independent Gaussian distributed complex vector fields [30]. This is the assumption under which the previous section was discussed. When the underlying fields are Gaussian distributed, the joint probability of the complex fields is given by [7]

$$p\left(E_x^{'}, E_x^{''}, E_y^{'}, E_y^{''}\right) = \frac{1}{4\pi\sigma^4}\exp\left\{-\frac{\left(E_x^{'}\right)^2 + \left(E_x^{''}\right)^2 + \left(E_y^{'}\right)^2 + \left(E_y^{''}\right)^2}{2\sigma^2}\right\}, \qquad (2.16)$$

where $E'_{x,y}$ and $E''_{x,y}$ are the real and imaginary parts of the complex field respectively and σ is an arbitrary constant. However, this is not the only underlying field distribution that can be described as Type I unpolarized light. It is possible to create a distribution that is still invariant to rotations of the coordinate axis on the sphere but is not due to independent Gaussian distributed complex fields.

For purposes of visualizing distributions on the observable polarization sphere, the probability distributions of polarization states will be defined in terms of the spherical coordinate angles 2α, and Δ, with the relation

$$S_1 = r\cos(2\alpha), \tag{2.17}$$

$$S_2 = r\sin(2\alpha)\cos(\Delta), \tag{2.18}$$

$$S_3 = r\sin(2\alpha)\sin(\Delta), \tag{2.19}$$

where 2α is bound between 0 and π and Δ is the phase difference between the two orthogonal directions modulo 2π ($\Delta \in [0,2\pi]$). Under the assumption of pure states of polarizations, $r = 1$. The uniform distribution of polarization states, one that includes the distribution of independent Gaussian fields is defined as

$$p(r, 2\alpha, \Delta) = \delta(r-1)\frac{1}{2\pi}\frac{\sin(2\alpha)}{2}. \tag{2.20}$$

An example of this distribution and of Type I unpolarized light can be seen in Figure 2-4a.

There also exist cases in which the polarization states do not follow a Gaussian statistical model yet remain globally unpolarized. Gaussian statistics are completely specified by second-order moments and give little information about the underlying scattering systems, while non-Gaussian distributions are not limited to this restriction [33,34]. These distributions lead to additional types of unpolarized fields. The second type of unpolarized light requires the statistical properties of the distribution to be invariant to the introduction of a half-wave plate and the reversal of the direction of propagation, but no longer invariant to the introduction of an arbitrary retardation [35]. This means that the distribution is invariant to rotation about the s_3 axis and symmetric about the s_1, and s_2 plane. Such is the case of a uniform distribution of all linear states

$$p(r,2\alpha,\Delta)=\delta(r-1)\frac{\sin(2\alpha)}{2}\frac{1}{2}\left[\delta(\Delta)+\delta(\Delta-\pi)\right], \tag{2.21}$$

as seen in Figure 2-4b.

The final type of unpolarized light discussed here, Type III, is still invariant to the direction of propagation but is now dependent on introductions of either an arbitrary retardation or an arbitrarily oriented half-wave plate [35]. This is basically a Type II unpolarized light with the introduction of an appropriate retardation. A simple representation of Type III would be the distribution of all states with $S_1 = 0$, or a banded structure that is only invariant to the inversion of S_3 to $-S_3$;

$$p(r,2\alpha)=\delta(r-1)\frac{1}{2\pi}\frac{1}{a}rect\left[\frac{1}{a}\left(2\alpha-\frac{\pi}{2}\right)\right], \tag{2.22}$$

where a is some arbitrary constant bound in the interval $[0,\pi]$. An example of this distribution is illustrated in Figure 2-4c.

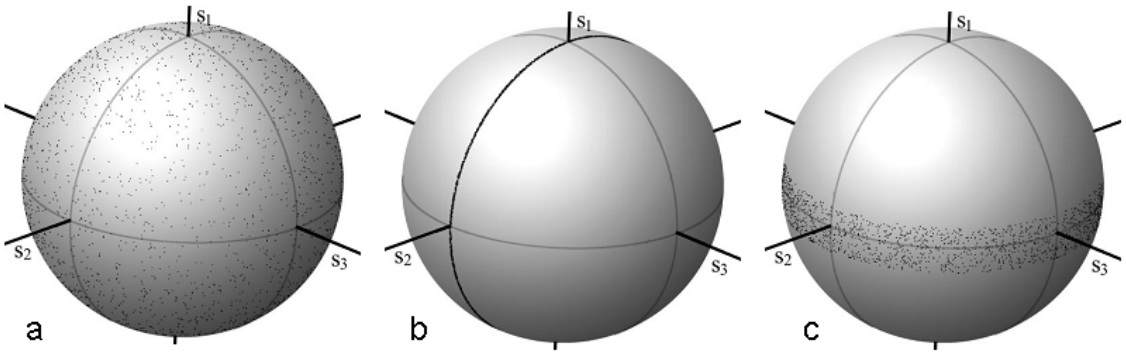

Figure 2-4: (a) Example of Type I unpolarized; uniform distribution. (b) Example of Type II unpolarized; all linear states. (c) Example of Type III unpolarized; distribution about $s_1 = 0$.

2.5 Higher-order Field Correlations

Although the distribution of states on the observable polarization sphere provides a simple qualitative means to assess different types of unpolarized light, these distributions can also be quantified with Stokes vector element correlations, fourth-order field correlations. In the case of Gaussian distributed fields, the fourth-order correlations factorize into terms of the second-order correlations. When the field distribution is non-Gaussian, then the correlations do not factorize and they carry specific information pertaining to the field distribution. The correlations between Stokes elements follow the form $\langle s_i s_j \rangle$, which easily relates to the shape information of the polarization distribution on the observable polarization sphere. Theoretical examples acquired from the distributions (Eqs. 2.20,2.21,2.22) defining the different types of unpolarized light are listed in Figure 2-5.

Type	(a) Average Stokes Vector	(b) Average Intensities	(c) Stokes Vector Element Autocorrelation	(d) Stokes Vector Element Crosscorrelations
I	$\langle S\rangle = \begin{pmatrix}1\\0\\0\\0\end{pmatrix}$	$\langle I_x\rangle = 2\sigma^2$ $\langle I_y\rangle = 2\sigma^2$ $\langle I_t\rangle = 4\sigma^2$	$\langle s_1^2\rangle = \frac{1}{3}$ $\langle s_2^2\rangle = \frac{1}{3}$ $\langle s_3^2\rangle = \frac{1}{3}$	$\langle s_1 s_2\rangle = 0$ $\langle s_1 s_3\rangle = 0$ $\langle s_2 s_3\rangle = 0$
II	$\langle S\rangle = \begin{pmatrix}1\\0\\0\\0\end{pmatrix}$	$\langle I_x\rangle = 2\sigma^2$ $\langle I_y\rangle = 2\sigma^2$ $\langle I_t\rangle = 4\sigma^2$	$\langle s_1^2\rangle = 0.273$ $\langle s_2^2\rangle = 0.3635$ $\langle s_3^2\rangle = 0.3635$	$\langle s_1 s_2\rangle = 0$ $\langle s_1 s_3\rangle = 0$ $\langle s_2 s_3\rangle = 0$
III	$\langle S\rangle = \begin{pmatrix}1\\0\\0\\0\end{pmatrix}$	$\langle I_x\rangle = 2\sigma^2$ $\langle I_y\rangle = 2\sigma^2$ $\langle I_t\rangle = 4\sigma^2$	$\langle s_1^2\rangle = \frac{1}{2}$ $\langle s_2^2\rangle = \frac{1}{2}$ $\langle s_3^2\rangle = 0$	$\langle s_1 s_2\rangle = 0$ $\langle s_1 s_3\rangle = 0$ $\langle s_2 s_3\rangle = 0$

Figure 2-5: Statistical characteristics of globally unpolarized light: (a) the average Stokes vector, (b) the average intensity along the two orthogonal directions defining the reference frame and the average total intensity (σ is an arbitrary constant), (c) the Stoke vector element auto-correlations, and (d) the Stokes vector element cross-correlations. The values of the quantities in (a) and (b) are independent of reference frame, the choice of right versus left handed circular polarization, and they are invariant to the introduction of an arbitrary retardation. The values in (c) and (d) for Type II and III unpolarized light depend on the specific distributions chosen. Under an arbitrary retardation, introduction of a half-wave plate, or reversal of direction of propagation, the resulting values of these six correlations in the new coordinates of the observable polarization sphere will be linear combinations of the original values.

It was found that for strong multiply scattering media resulting in a uniform distribution of all polarization states, the average Stokes elements and cross-correlations were zero $\left(\langle s_1\rangle = \langle s_2\rangle = \langle s_3\rangle = \langle s_1 s_2\rangle = \langle s_1 s_3\rangle = \langle s_2 s_3\rangle = 0\right)$ while the auto-correlations were 1/3 $\left(\langle s_1^2\rangle = \langle s_2^2\rangle = \langle s_3^2\rangle = 1/3\right)$ [36]. Deviations from these correlations give insight to the possible types of scattering particles and their arrangement. Experimental results showed that cylindrical

(plate-like) particles on the exiting surface of a bulk scattering material acted as partial linear polarizers with random orientations. This led to a suppression of circular states. Whereas for an optical depolarizer, the diagonal linear states (s_2) were suppressed. This was in contrast to spherical particles, which showed a much more uniform distribution. These experimental results from Ref. [36] are shown in Figure 2-6. These correlations begin to form the basis of using polarization to solve a stochastic inverse problem, inferring particle shape in a scattering medium.

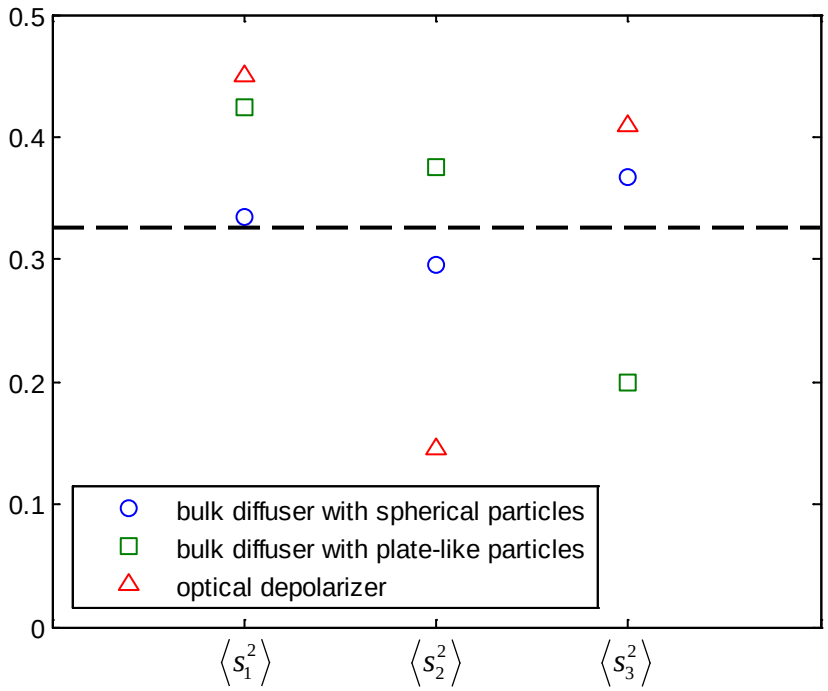

Figure 2-6: Experimental results of Stokes vector element correlations. The dashed line indicates the expected values for Gaussian-distributed fields, while the symbols are larger than the standard deviation between measurements of similar samples.

Stokes element correlations provide means to quantify the polarization fluctuations of random fields. An additional means is to look at fourth-order point-pair correlations. These

correlations compare the polarization similarity of two distinct points. The length between points can either be spatial or temporal and gives insight into the length scales associated with a random field. There are a few means of measuring the similarity of polarization states that manifest from spatial variation of polarization and coherence properties. There is the beam coherence polarization matrix, a generalization of the polarization tensor that largely ignores the direction of propagation [37]. The recently developed unified theory of coherence and polarization proposed by Wolf addresses the propagation of these properties along the beam [38]. The generalized degree of polarization measures how similar the global polarization is across a beam [39]. A more recent comprehensive quantity that measures polarization similarity between two arbitrary points (r_1 and r_2) is the complex degree of mutual polarization (CDMP) [40]. It is invariant to coordinate frame and reduces down to the classic definition of the degree of polarization when $r_1 = r_2$. It is a complex quantity containing information in both its magnitude and phase. Under the assumption of a fully correlated and locally fully polarized field, the CDMP simplifies to

$$V^2(r_1, r_2) = \frac{\left(E_x^*(r_1)E_x(r_2) + E_y^*(r_1)E_y(r_2)\right)^2}{\left(E_x^*(r_1)E_x(r_1) + E_y^*(r_1)E_y(r_1)\right)\left(E_x^*(r_2)E_x(r_2) + E_y^*(r_2)E_y(r_2)\right)}. \quad (2.23)$$

The CDMP expresses the relation between polarimetric quantities at two points in terms of measurable quantities. The CDMP can be thought of as the distance between polarization states on the observable polarization sphere. The value is 1 when the two states are the same and 0 when they are orthogonal. When one state is horizontal linear and the other is 45 degree linear, then $\left|V^2(r_1, r_2)\right| = 1/2$ (half-way around the sphere). The same is true when calculating the CDMP

of a linear state with a circular state. The CDMP is a good additional measure of polarization fluctuations and polarization length scales as it examines how the polarization state differs from a known reference.

CHAPTER 3: TRADITIONAL APPROACHS TO SCATTERING INVERSE PROBLEMS

The light scattering phenomenon can generally be broken down to a simple direct problem, scattering from a single particle. This requires solving and quantifying the entire scattering process once the scattering medium is known. Though, in time the particles may move, or there may exist a large number of scattering events for an individual photon, i.e. multiple scattering. The fluctuations that arise from this scattering can be manipulated or used to infer information about the scatterers in the medium or general properties of the medium on a whole. This is solving the inverse scattering problem, a complex stochastic problem with no analytic solution. This chapter will discuss a number of methods that are currently being used to solve different inverse problems, such as diffuse imaging, material flow, particle size and material diffusion.

3.1 Speckle Contrast Imaging

A type of imaging that exploits the presence of speckle fluctuations is known as laser speckle contrast imaging. As mentioned before, fully developed speckle has unity intensity contrast. A number of influences can cause the contrast to reduce including the addition of uncorrelated speckle patterns. The movement of the medium under examination causes the speckles to change in time, creating a number of uncorrelated patterns that reduce the contrast. By selectively calculating the contrast over small areas across the entire speckle image, the objects of high movement reveal themselves in the final contrast image [41]. This technique has been used in biology as a means to detect and visualize blood perfusion in tissue [42–45].

The contrast images are based on particle movement and that the speckle contrast is related to the particle speed. Thinking of the dynamic speckles in the time domain and associated temporal fluctuations, an important value is the decorrelation time. Based on Lorentzian or Gaussian distributions, the decorrelation time τ_c relates to the particle decorrelation velocity υ_c by [46]

$$\upsilon_c = \frac{\lambda}{2\pi\tau_c}. \tag{3.1}$$

In turn, the speckle contrast can be described in terms of the decorrelation time and the exposure time T. Assuming a Lorentzian velocity distribution the contrast is defined as [47]

$$C = \sqrt{\frac{\tau_c}{2T}\left(1 - exp(\left(-\frac{2T}{\tau_c}\right)\right)}. \tag{3.2}$$

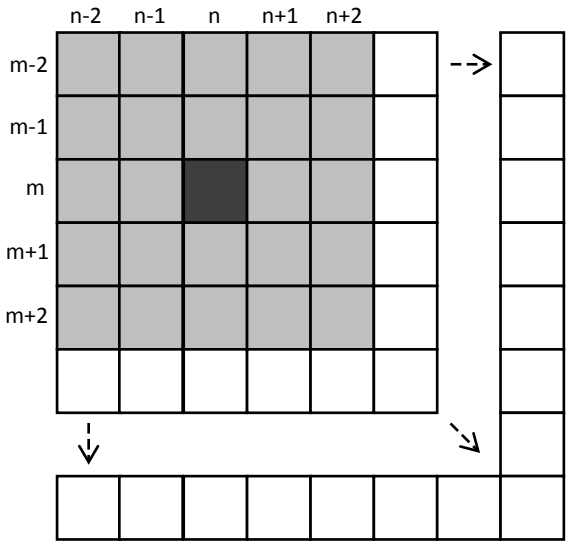

Figure 3-1: Schematic overview of LASCA contrast calculation. The contrast in pixel (m, n) (dark gray) is calculated from the surrounding pixels (light gray).

Based upon the relation between particle velocity/decorrelation time and the speckle contrast, a number of different analysis methods have been developed to exploit this relation and image particle flow. Building upon early experiments of double-exposure speckle photography [48,49], Briers and Webster developed a digital single speckle photography known as laser speckle contrast analysis (LASCA) [42,46]. The principle of LASCA is to examine the speckles only a small subset at a time and to calculate the speckle contrast of each subset (Figure 3-1). This is basically a spatial integration across the image and thus results in lost resolution. Once the contrast image has been calculated, the areas of high particle movement should show themselves as low contrast. LASCA has been used quite effectively and non-invasively to image blood vessels under the skin and has now seen expanded use within dermatology and ophthalmology [50]. LASCA is inexpensive and fast but can also be controlled and optimized for the current task to help counteract some of its limitations. The sensitivity can be controlled by adjusting the integration/exposure time. In addition to increased signal with increased exposure

time, the speckle contrast noise also increases. There may be optimal exposure times for the task at hand, such as around 5 ms in rodent brains [45]. The speckle size should also be matched to the camera pixel size and was found that when the two are on the same order, error is minimized [45,51].

Since LASCA is a measurement over a group of pixels, effectively ``binning'' the image, there is a loss in resolution. To counteract this, the method of laser speckle imaging (LSI) was proposed, which instead of integrating spatially, instead integrates temporally [52]. It essentially calculates the contrast of one pixel over many images, instead of several pixels from one image. This method is of course much slower than LASCA in that it requires an ensemble of measurements. Unfortunately, due to the nature of this calculation, areas of no flow and areas of high flow both appear as regions with low contrast. This makes LSI an unsuitable method for samples that have non-dynamic regions.

Overall, speckle contrast imaging is an effective method to view particle flow, especially blood flow in diffuse scattering media. Whether time is a necessity (LASCA) or resolution (LSI), the methods depend on the dynamic intensity fluctuations of speckles.

3.2 Scattering Measurement Techniques

When considering the scattered light from a complex medium, ultimately one goal is to learn about the medium. When the medium is not just a simple case of single particles scattering, you can turn to a number of light scattering techniques. Several dynamic systems/media exist such as solids, gels, solutions of suspended particles, and biological tissues that have either very complex structures or contain particles that shift and move causing intensity fluctuations. The use of laser light is quite useful in quantifying the displacements of particles in a time-resolved

manner. This technique is known as dynamic light scattering (DLS) and is capable of retrieving the mean square displacement from the temporal fluctuations and infer structural properties of the dispersive medium [53].

3.2.1 Dynamic Light Scattering

In principle, monochromatic light is incident upon the dynamic medium and the scattered light is collected with an autocorrelator. In conjunction with the autocorrelator, DLS depends upon a modeled system, and one common model to address the dynamics of the particles is that the movement is due to Brownian motion. As the particles experience displacement, the optical field undergoes phase changes leading to fluctuations in intensity. Assuming the particle displacement follows a Gaussian distribution, a final scattering function can be found

$$F(q,t) = exp\left[\frac{-q^2\left\langle \Delta R^2(t)\right\rangle}{6}\right], \tag{3.3}$$

where $\left\langle \Delta R^2(t)\right\rangle$ is the mean square displacement and q is the scattering vector, $q = (4\pi/\lambda)sin(\theta)$. For Brownian motion, $\left\langle \Delta R^2(t)\right\rangle$ relates to the diffusion coefficient of suspended particles

$$\left\langle \Delta R^2(t)\right\rangle = 6Dt, \tag{3.4}$$

which in turn relates to particle size a and viscosity η

$$D = \frac{k_B T}{6\pi\eta a}. \tag{3.5}$$

DLS is useful to not only quantify the motion of particles but also to infer their size.

As alluded to previously, single scattering is a much simpler situation to address, but only applies when the average dimensions of the medium are smaller than the scattering mean free path l_s. When the light scatters through a medium at longer distances, many scattering events occur, leading to a complex problem that must be solved statistically. DLS applies for weakly scattering light, and only works under the assumption that the light scatters but once before detection.

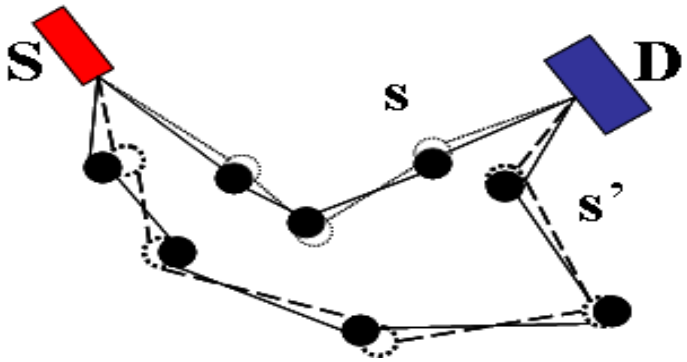

Figure 3-2: Schematic of diffusing wave spectroscopy

3.2.2 Diffusing Wave Spectroscopy

Diffusing wave spectroscopy (DWS) is a method that extends DLS to strongly, multiple scattering media [54,55]. Again, like in DLS, the temporal intensity fluctuations are measured within a speckle. Following the schematic in Figure 3-2, instead of single scattering events, in DWS the field autocorrelation measurement is an average over all possible angles and scattering paths. When assuming a large number of scattering events, the path-length followed is $s = n * l_s$ and relates to the transport mean free path l^* by

$$l^* = \frac{2k_0^2 l_s}{\langle q^2 \rangle}. \tag{3.6}$$

DWS involves an average over all possible path-lengths and is weighted by the probability density function $P(s)$, the probability that photons traveled a path-length s. DWS is a useful measuring technique within the multiple scattering regime and continues to be useful in dynamic imaging of colloidal suspensions and fluctuating media [56,57] or even expanded to describe the crossover between single-scattering and diffusive regimes [58].

3.2.3 Optical Path-length Spectroscopy

An extension of DWS is the method of optical path-length spectroscopy (OPS) and its ability to obtain $P(s)$ independently from the diffusion model [59,60]. Through ensemble averaging, using OPS one can calculate mean statistical properties such as l^* and the diffusion coefficient. Using the principles of low coherence interferometry (LCI) [61], OPS directly infers the path-length distribution P(s) of waves scattered from random media. LCI has shown to be quite useful in biomedical imaging as the short temporal coherence provides a greater depth resolution and is also commonly referred to as optical coherence tomography [62,63]. In the case of strong multiple scattering, the use of monochromatic light gives rise to sharp transitions of min/max intensity values, the presence of speckles. When using a low-coherence source, such as a broadband LED, the intensity min/max transitions are of low contrast, and give a kind of "smeared" speckle.

The experimental OPS method uses radiation with a short coherence length and an envelope detection of the interferometric signal provides a direct measure of scattering contributions with specified path-lengths. The OPS measurements are based on fiber optic

arrangements that permit different modalities for injecting light into and collecting reflected light from a scattering medium. The configuration can be monostatic, where the same fiber acts as both the source and detector or bistatic. In the bistatic configuration the injection and detection points are separated by an adjustable distance Δ allowing for an experimental control over the volume of interaction. The OPS signal consists of backscattering intensity contributions from a combination of closed loops all with the same optical path-length. From the shape of the curve, relating these backscattered intensities with corresponding path-lengths, the transport mean free path can be determined.

Even when using a low-coherence source, low contrast "smeared" speckles still occur, so an ensemble average over different realizations of the wave-medium interaction is acquired to achieve the optical path-length distribution. The $P(s)$ acquired is over a large range of path-lengths, from the single scattering regimes to regimes of complete diffusion. Figure 3-3 shows an example $P(s)$ curve acquired from OPS. The inset demonstrates how the longer path-lengths penetrate deeper into the medium and sample a larger volume.

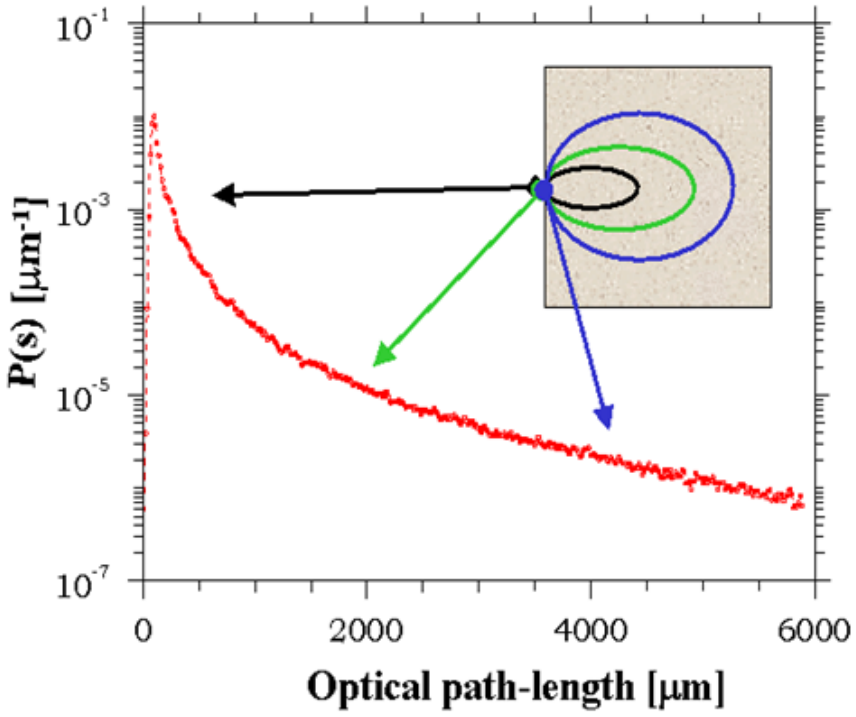

Figure 3-3: Typical optical path-length distribution and its depth penetration into the medium.

The diffusively backscattering energy flux is calculated by applying a time-dependent diffusion approach. The diffuse energy density satisfies the diffusion equation under the assumption of negligible absorption. The diffusion coefficient D is related to the transport mean-free path l^* with the relation $D = (vl^*)/3$. With an average energy transport velocity v, the energy flux detected in OPS is

$$J(s) = (4\pi l^*/3)^{-3/2} z_e v s^{-5/2} exp\left(-\frac{3z_e^2}{4sl^*}\right), \tag{3.7}$$

where z_e is the so-called extrapolation length [60].

From the experimentally obtained $P(s)$ curves, the distributions are fitted with the relation seen in Eq. 3.7 to infer the value of l^*. This method of OPS has been demonstrated in the past to measure the transport mean free paths of water suspended polystyrene microspheres as seen in Ref. [59] and Figure 3-4.

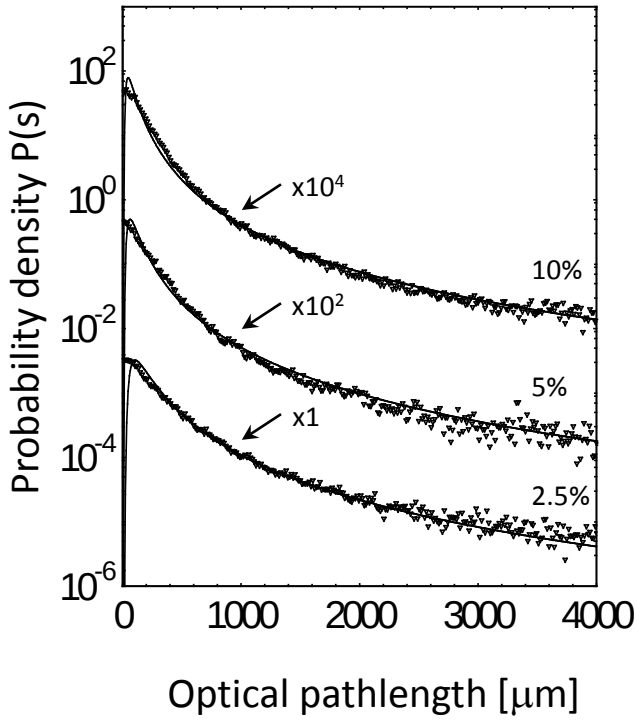

Figure 3-4: Optical path-length distribution for suspensions of microspheres with different volume fractions.

3.3 Fluctuation Analysis of OPS

Both DWS and OPS depend on ensemble averages to infer mean statistical properties of scattering media. Unfortunately, by taking the ensemble average of different material realizations of a medium, any information relating the particular material configuration is lost. The transport mean free path is a quantity that depends on the number density of scatterers as well as size and

shape, $l^* = [N\sigma_s(1-g)]^{-1}$. This gives rise to the possibility of having two media that are described by the same diffusion coefficient, and thus have the same path-length distribution curves in average. The probability distribution $p_\alpha(s)$ resulting from a single realization α is unique and is a sampling, or a peek into the configuration and construction of a particular medium. Within OPS, it is possible to examine the $p_\alpha(s)$ fluctuations from one realization to the next at a particular path-length to distinguish between two media described by the same diffusion coefficient [64].

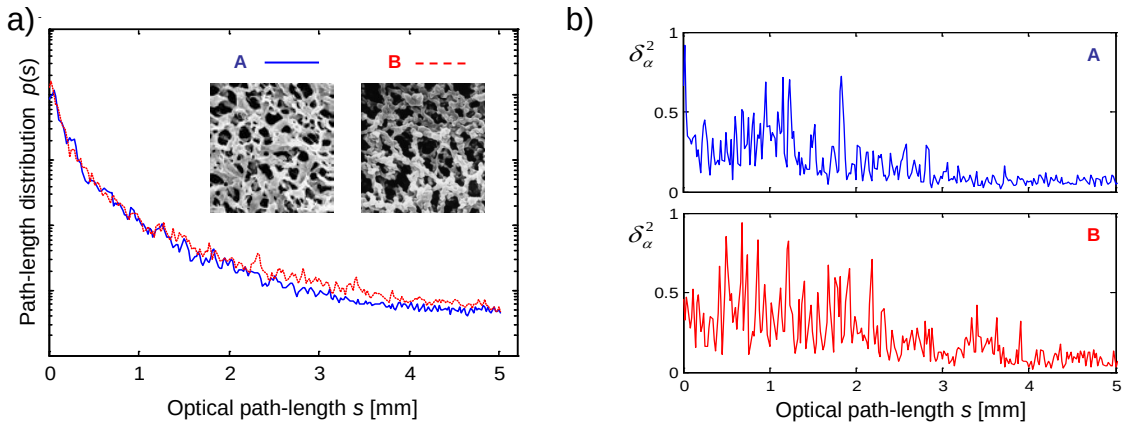

Figure 3-5: (a) The averaged backscattered intensities for medium A (blue solid line) and medium B (red dashed line). The insets show typical micrographs of the materials examined. (b) Typical mean square fluctuations $\delta_\alpha^2(s,\xi_\alpha)$ of path-length distributions.

An example of two such media with the same l^* can be seen in Figure 3-5a. Though in average the two path-length distributions coincide, their individual path-length distributions resulting from a single realization are quite different and unique. The $p_\alpha(s)$ curve resulting from a single realization α can be simply visualized as fluctuations from the mean-statistical distribution. The two media in Figure 3-5a may have the same mean properties but differ greatly

in their fluctuations from the average $\delta_\alpha^2(s,\xi_\alpha)$, where ξ_α is a configuration function describing the particular morphology of realization α. These deviations from the average are more pronounced in one medium over the other, as seen from the mean square fluctuations in Figure 3-5b.

Evidently, the random function $p_\alpha(s)$ displays non-stationary fluctuations in s and also shows differences from one material realization to another. There are many ways in which the two-dimensional statistical characteristics of $p_\alpha(s)$ can be quantified. Of course, a simple averaging over α will provide a path-length distribution $p(s) = f(s,D)$ which corresponds to the ensemble average. For a single realization α on the other hand, higher order moments of the fluctuations in $p_\alpha(s)$ can be evaluated. Even though $p_\alpha(s)$ is non-stationary in s, one can still calculate simple estimators such as the variance of the fluctuations along s:

$$V_\alpha(\xi_\alpha) = \int \delta_\alpha^2(s,\xi_\alpha)\,ds - \left|\int \delta_\alpha(s,\xi_\alpha)\,ds\right|^2. \tag{3.8}$$

However, this simple estimate is inadequate because $\delta_\alpha(s,\xi_\alpha)$ is a zero-mean random function and, consequently, a unique and meaningful normalization is difficult to define.

As the deviation $\delta_\alpha^2(s,\xi_\alpha)$ from the ensemble average can be regarded as a form of disorder, we can choose to examine its variance in terms of the Shannon information entropy [65]:

$$H_\alpha(s_1,s_2) = -\int_{s_1}^{s_2} \frac{\delta_\alpha^2(s,\xi_\alpha)}{\int_{s_1}^{s_2}\delta_\alpha^2(s,\xi_\alpha)\,ds} \log\left(\frac{\delta_\alpha^2(s,\xi_\alpha)}{\int_{s_1}^{s_2}\delta_\alpha^2(s,\xi_\alpha)\,ds}\right) ds. \tag{3.9}$$

In Eq. (3.9), we define this finite scale entropy to account for realistic situations of any measurement that extends over a finite range $[s_1, s_2]$. Furthermore, the finite scale entropy can be normalized to its maximum allowable value for the entire range $S = s_2 - s_1$ as

$$h_\alpha(s_1, s_2) = -H_\alpha(s_1, s_2) / \log\left(\frac{1}{S}\right). \tag{3.10}$$

Of course, the normalized entropy $h_\alpha(s_1, s_2)$ will still vary from realization to realization and one can further build its average $\overline{h_\alpha(s_1, s_2)}$ over the number of realizations available. Being constructed in terms of the specific fluctuations of each realization α, this average is a comprehensive measure of the overall fluctuations. It depends directly upon N and the configuration of the scatterers.

This can be expanded in more detail to a situation where the scale of available path-lengths is varied. In practice, this amounts to controlling the size of the interaction volume which can be implemented in a two fiber bistatic OPS measurement. By increasing the source-detector separation Δ, the interaction volume is enlarged while enforcing a minimum path-length. According to our notation in Eq. (3.9), this amounts to setting the lower path-length limit at $s_1 = \Delta$ and the upper one at $s_2 = \Delta + S$. Here S denotes the value of the total span of path-lengths available in the measurement; S is constant in our experiments. Subsequent normalization and averaging over different realizations was performed following the procedure outlined by Eq. (3.10). In Figure 3-6 we present the values of the normalized scale dependent entropy $\overline{h_\alpha(\Delta)}$ averaged over ten realizations of disorder for both media examined.

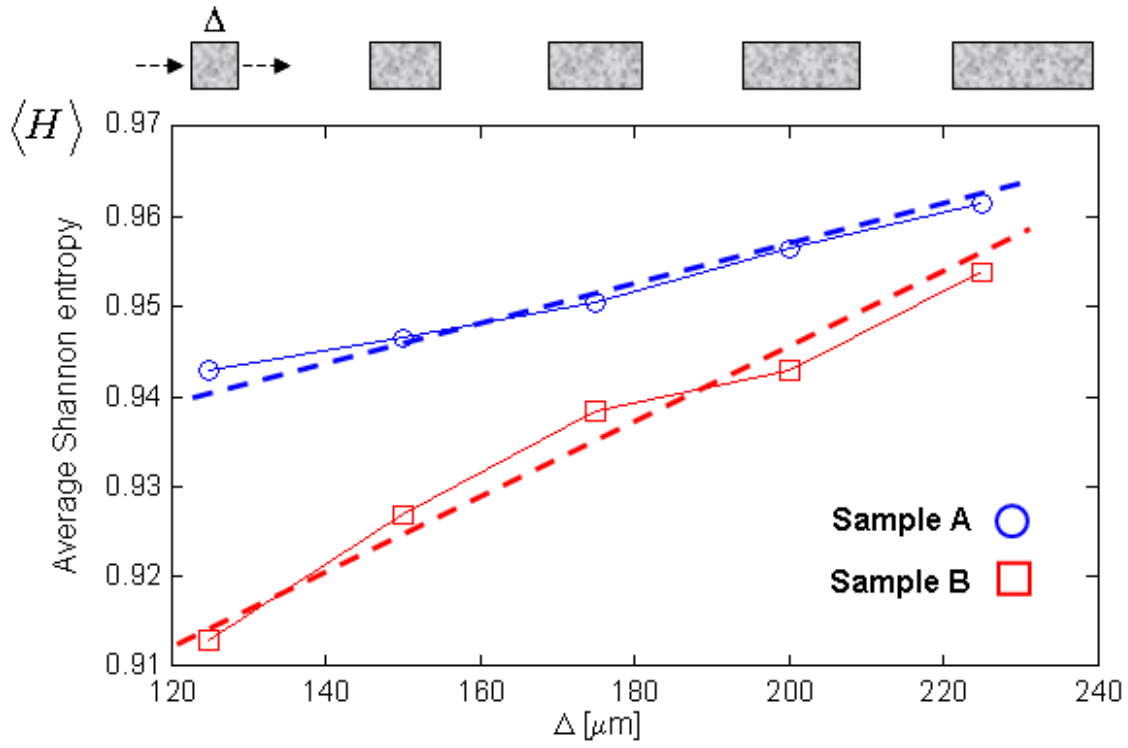

Figure 3-6: Average normalized entropy $\overline{h_\alpha(\Delta)}$ for medium A (blue circles) and medium B (red boxes) for increasing volumes of interaction.

As can be seen for both media, when the interaction volume increases, the entropy increases as expected because in all realizations α, $\delta_\alpha^2(s,\xi_\alpha)$ is a non-stationary process, and its fluctuations decrease at larger S. The absolute values and the rate of increase for $\overline{h_\alpha(\Delta)}$ however are medium specific.

Two main observations are in place. First, we notice the higher values of the entropy for medium A. This is the result of a higher number density of scattering centers which determines a larger number of possible optical paths having a given length s. Therefore, there are smaller fluctuations in $\delta_\alpha^2(s,\xi_\alpha)$ as discussed before and, consequently, the entropy tends toward its value corresponding to an infinite number of possible trajectories of length s.

The second observation relates to the different rates of entropy increase as suggested by the dashed lines in Figure 3-6. This behavior can be understood by realizing that a certain path-length s can be reached through a different number m of scattering events. For independent scattering, the joint distribution $p(s,m)$ of such a process is Poissonian and the cumulative probability of scattering orders up to M that contribute to paths of length s is described, in average, by a universal cumulative distribution function $p(s,M)$ [8]. This cumulative distribution increases fast for low values of M and tends to saturate for higher scattering orders. In one realization where the interaction volume is finite, the maximum scattering order M contributing to a certain s is essentially determined by the number density of available scattering centers. Thus, processes involving different number densities will in fact experience different regions of the cumulative distribution function. For the sparser medium B, a change in M results in a faster increase of the corresponding values of $p(s,M)$ and, consequently, a faster decrease in the possible fluctuations. Because the entropy is a measure of magnitude of these fluctuations, it follows that the medium B should be characterized by a faster rate of entropy increase as can be seen in Figure 3-6. As a result, in spite of being described in average by the same diffusion coefficient D, the two media can be discriminated based on their corresponding densities of scattering regions. This information was not available in the ensemble average.

There are a number of ways to quantify these fluctuations but the result is clear, examining the intensity fluctuations from the mean behavior of a medium provides additional insight into the structure and configuration of the medium.

3.4 Summary

There are a number of methods that take advantage of the fluctuations in intensity that result from light matter interaction. This chapter focused mostly on methods that focused on the scalar intensity properties and required an ensemble of realizations. These methods can be used for imaging purposes (LASCA) or for assessing the diffusive properties of a medium (DLS, OPS).

We also demonstrated that a single realization of light matter interaction thoroughly samples the medium yet gives a very complicated result. By closely examining the intensity fluctuations from subsequent realizations in OPS experiments, we were able to differentiate between two scattering media that have very similar diffusive properties in average. The process of examining the information entropy is not limited intensity fluctuations but can be used to apply to any non-stationary fluctuating process.

As we will see in the following chapter, it is very useful to be able to more thoroughly examine results from a single realization. There are a number of physical instances where one does not have access to an ensemble of realizations such as in an ultrafast one-time occurrence. Or there may be situations in which the process of acquiring a single realization is too long and cumbersome to acquire many.

CHAPTER 4: STOCHASTIC PROBLEMS GOING BEYOND ENSEMBLE AVERAGES

Most of the traditional approaches, including the ones highlighted in Chapter 3, rely upon an ensemble average of realizations to quantitatively solve the material properties. In many cases, the material properties are statistical in nature and are actually average properties, such as the transport mean free path and diffusion length. As shown in Section 3.3, there is value in closely examining the underlying fluctuations that occur from one realization to the next. Even fluctuations from one single realization, though complex and difficult to parse, give insight into the nature of the light matter interaction. In this section, a number of approaches to the analysis of single realizations of light-matter interaction are discussed. Especially in the context of polarization, it is demonstrated that a number of material properties such as scattering regime, transport mean free path and relative scatterer size can be determined from one single realization of the interaction.

4.1 Polarization Length Scales in Different Scattering Regimes

It is possible that polarization length scales associated with scattered fields can be different from the associated intensity length scales. The complex degree of mutual polarization (CDMP) provides a simple measure to calculate the polarization similarity between two points, and thus can be used to find an associated polarization length scale [40]. In a typical speckle pattern resulting from strong multiple scattering, the associated intensity length scale is about the size of an average speckle, the extent of the C_1 correlation. The polarization length scale is also about the size of a speckle demonstrating that there is very little correlation between the state of polarization from speckle to speckle, as can be seen in Figure 4-1a. The polarization state

changes a little after every scattering event and due to a large number of scattering events, the interferences from the multiple paths create unique polarization states for each individual speckle. This is the situation for Type I depolarization as described in Section 2.4. An optical depolarizer depolarizes the light without modulating the intensity, which is an example of when the polarization length scale is shorter than the intensity. The optical depolarizer is basically a grid of differently oriented wave plates such that a sufficiently large beam of light that passes through becomes globally unpolarized. Whereas the intensity stays constant, as seen in Figure 4-1b, the polarization fluctuates on a scale associated with the periodicity of the depolarizer. The polarization length is actually two-fold: along one axis the polarization fluctuates yet along an orthogonal axis, the polarization remains constant, seen in the inset of Figure 4-1b.

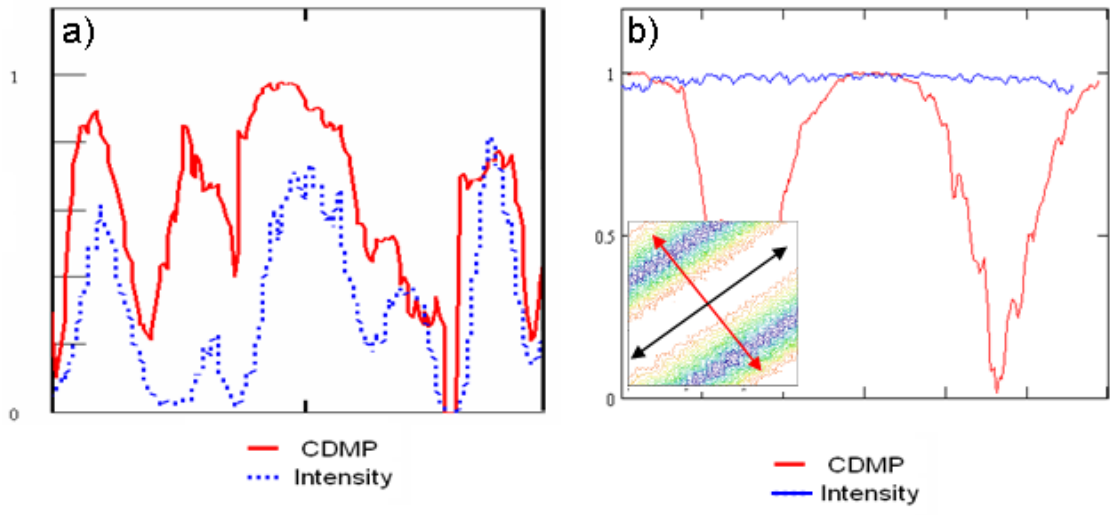

Figure 4-1: Examples of different length scales in polarization and intensity. (a) For a random speckle field, intensity and CDMP fluctuations follow each other on the length scale of a speckle. (b) For an optical depolarizer, polarization follows a periodic fluctuation while intensity remains constant. Inset show 2-D CDMP map of the depolarizer.

4.1.1 The CDMP in Random Electromagnetic Fields

A simple way to describe the intensity speckles is to consider the superposition of waves originating from discrete scattering centers. Different scattering regimes may vary from "single scattering" specific to mostly surface scattering to different degrees of multiple scattering characteristic to the interaction with three-dimensionally disordered media. When one single polarization component is analyzed, i.e. when the speckle field is measured through a polarizer, the intensity contrast often reaches unity. This is the case of the so-called fully developed speckle pattern, a manifestation of interference between a large number of wavelets with uniformly distributed random phases. This is a rather universal behavior present in scattering from a variety of media ranging from metallic rough surfaces to diffusive materials.

However, the distribution of polarization states in random electromagnetic fields (REFs) is much richer and non-universal properties are to be expected. Most importantly, it is anticipated that the polarization properties of REFs corresponding to different scatting regimes will depend greatly on the strength of the scattering process. For instance, it is likely that when the wave interaction is dominated by single scattering processes, a fully developed speckle pattern will occur but the REF polarization will strongly resemble the incident state of polarization. On the other hand, when the interaction is subject to strong multiple scattering, the scattered field remains locally fully polarized but its state of polarization will vary spatially. When the scattering process is completely diffusive, universal distributions emerge for the polarization parameters [20,30]. It is therefore of interest to examine in detail the relation between the degree (order) of scattering and the polarization properties of the resulting REF.

A number of studies and experiments have been aimed at characterizing scattered fields [30,66–72]. The fluctuations of one-dimensional speckles (1-D) and the global non-stationarities

of two-dimensional fields have been used to characterize specific properties of REFs [64,73]. In this section we will examine different means to discriminate between REFs originating from different scattering regimes. We will specifically focus on fields having similar global properties and discuss a number of high-order polarization correlations as means to assess the strength of different types of scattering.

One of the simplest methods to test for the depolarizing nature of the scattering of radiation of different degrees of coherence is to measure the degree of polarization (DoP) averaged over a large spatial scale. The DoP at a single point is

$$P(r_i) = \frac{\sqrt{S_1^2(r_i) + S_2^2(r_i) + S_3^2(r_i)}}{S_0(r_i)}, \tag{4.1}$$

but as stated before, this is of little interest when the incident radiation is fully coherent because the individual speckles are locally in pure states of polarization. But as the scales over which the averaging is performed grows, a scale dependent effective DoP can be defined as

$$\bar{P}_A(r) = \frac{\sqrt{\int_A S_1^2 dr + \int_A S_2^2 dr + \int_A S_3^2 dr}}{\int_A I dr}. \tag{4.2}$$

This scale dependent DoP approaches zero when the ensemble of polarization states are more randomly distributed. Section 2.4 pointed out that there are varying degrees and types in which a field can be considered globally unpolarized. The use of Stokes element correlations provided means of differentiating between the different types of unpolarized light. Unfortunately these correlations lose all spatial information in the case of a scattered field.

A simple experiment was designed to study the speckles produced at the surface of a random medium. The samples were illuminated with a linearly polarized laser at 488 nm. The sample surface was magnified and imaged onto a CCD, which collected the backscattered light. To fully resolve the speckles onto the CCD pixels, they were magnified 90x to about 80 μm.

We tested a number of media with varying degrees of surface roughness and volume scattering. The samples used correspond to a rough metallic surface (A) and three diffuse volume scattering media characterized by different transport mean free paths: a thin kaolin based diffuse coating (B), a cellulose membrane (C), and a polyvinylidene fluoride membrane (D). The scattered intensities were collected through a Stokes analyzer to achieve a spatially resolved full Stokes image. The polarization analyzer measures the full Stokes by means of the Fourier polarization method with the light passing through a rotating quarter wave plate and a stationary polarizer [32]. As the samples had varying strengths of scattering, the four samples had effective degrees of polarization $\bar{P}$ (calculated over the entire available scale) of 0.9811, 0.4951, 0.3056, and 0.2902 respectively. In general, the smaller values of $\bar{P}$ signify a stronger strength of scattering. As this is an ensemble calculation, the information about the relative polarizations of each speckle is practically lost. The effective DoP acts like the center of mass for the polarization states on the Poincare sphere where the polarization of the average state lies within the sphere and ignores the distribution of states as seen in Figure 4-2. In contrast, a point-pair correlation like CDMP measures the distance between two states on the sphere, it describes the shape of the distribution.

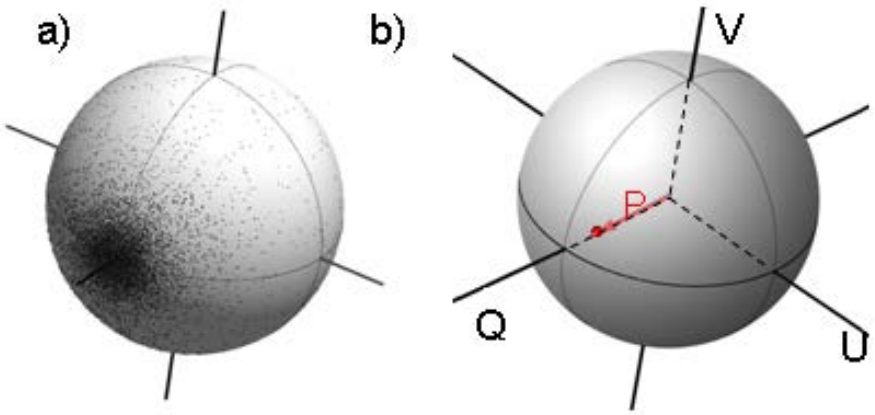

Figure 4-2: a) Distribution of polarization states on Poincare sphere. b) Both the average state of polarization and the degree of polarization are ensemble properties of the distribution of polarization states.

Through the use of CDMP, the spatial polarization similarity can be examined [74]. Each pixel in the image can be compared to a reference, in this case the chosen reference is the incident polarization state, and the resulting CDMP value can be used to encode the image of the scattered field. Because the CDMP is not an ensemble quantity, the CDMP can be calculated while maintaining spatial information. Figure 4-3 shows example CDMP maps calculated from the Stokes images acquired from the four samples.

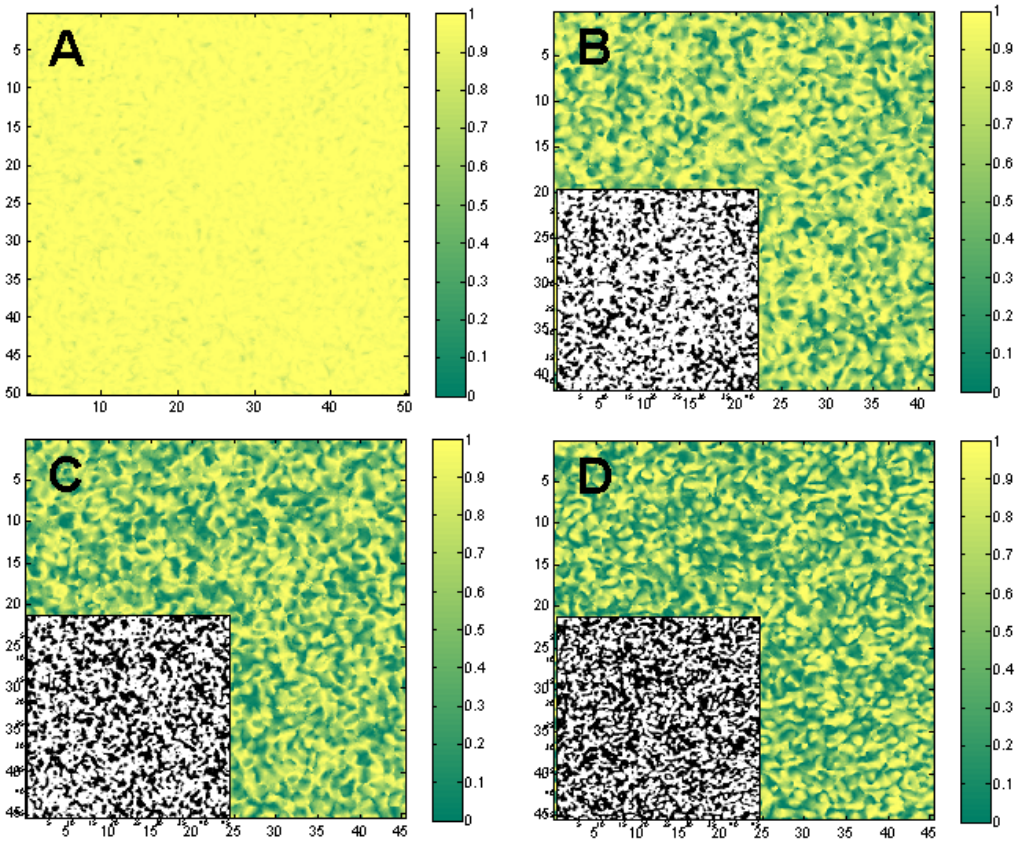

Figure 4-3: Map of CDMP values calculated from a known reference for the scattered light from samples representing different scattering regimes. Insets show a binary image of corresponding CDMP map thresholded at 0.5.

These CDMP maps give a 2-D spatial representation of the scattered light and their polarization similarity to the reference and thus some similarity to each other. The CDMP allows examination of the spatial distribution of states; comparing the Stokes measured in each pixel to a known reference. To make it even easier to see the number of pixels that show strong similarity to the reference state, binary images are shown in the insets, where all CDMP values above 0.5 are marked white. Though this is similar to the analysis performed in the enhanced backscattering regime described in section 4.4, the intensity fluctuations resolved here are

imaged on the surface, and are not angularly resolved. The speckle size is on the order of a wavelength and the speckles are directly related to the surface and volume features. Any surface discontinuities could potentially be resolved, as the scattered light has not yet propagated. This measurement configuration allows visualization of polarization correlations across the surface.

Sample A (a rough metallic surface) in Figure 4-3 shows very strong single scattering where all points are the same as the incident polarization state. This demonstrates very strong spatial correlation of the polarization. As the strength of multiple scattering increases, the spatial correlation of CDMP reduces as seen in images (B-D). Consider the random interference that generates this random field, the decrease in correlation from A to D is a result of the superposition of more and more contributions. This is similar to one or many more coherent sources with a number of different polarization states all contributing to each point in the scattered random electromagnetic field.

Another way to describe the polarization properties of the scattered field is to examine the distributions of CDMP across the image. These distributions (Figure 4-4) describe the shape that different polarization states form on the observable polarization sphere. Since the CDMP is a fourth-order correlation without ensemble averaging, it preserves the spatial information and allows these distributions to be calculated.

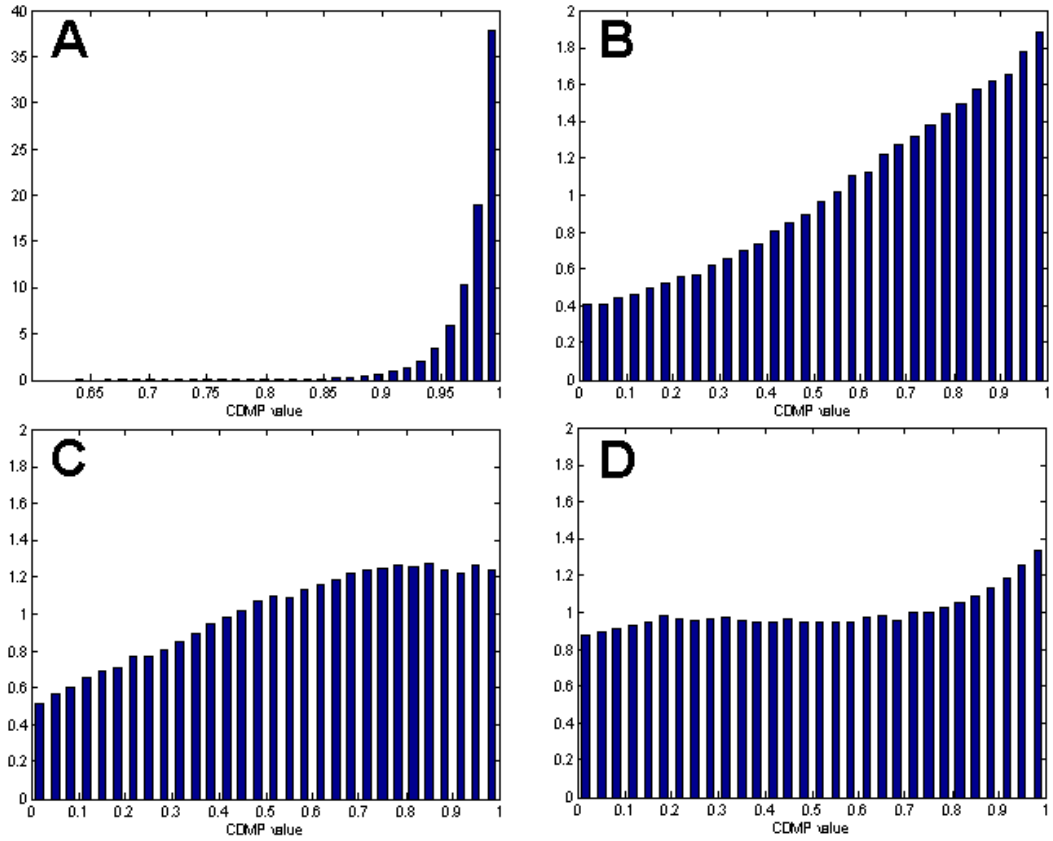

Figure 4-4: Probability distributions of the CDMP values for each sample. The reference is the incident linear polarization state.

The two extremes of distributions can be seen most readily in A and D. When the distribution favors CDMP values of one, this represents that all the points are the same as the reference state. For a completely single scattering sample, such as a mirror, this would result in a delta function centered at one. For the case of sample D, the distribution is more uniform, which corresponds to a more uniform coverage on the observable polarization sphere. The slight increase on the right-hand side of the distribution for sample D signifies a slight concentration around the reference polarization state. This preference to the incident state is due to the experimental reflection geometry, resulting in a small single scattering contribution. As noted

before, samples C and D before had similar effective degrees of polarization, but it is quite evident from the CDMP distributions that their coverage/shape on the sphere is quite different. It is also useful to examine the choice of other reference states. By choosing different reference states, the distributions will change accordingly. For example, the delta like distribution for sample A will shift toward zero as the reference moves away from the incident state.

To briefly comment on the information contained in these REF properties, it is known that a number of polarization memory effects are present at different levels of scattering [20,27,28]. There is an intimate dependence between the medium's structure and the polarimetric properties of the scattered field and, therefore, one can anticipate that the distribution of polarization states and their spatial correlation in a REF should reflect some of the morphological properties of the scattering media. Let us consider again the two samples that, in average, depolarize the light at essentially the same level, DoP $\approx$ 0.32, yet their structural morphology is quite different. From Figure 4-3 and Figure 4-4, one can clearly see that both the PDF of the corresponding CDMP maps and the sizes of the CDMP speckles are different for these samples. This is because the structural differences lead to different scattering strengths in these two media. To assess these differences we performed typical ensemble average measurements of enhanced back scattering (EBS) [75]. These measurements yielded different values of the transport mean free path: 8 and 7 μm for media C and D, respectively, as estimated from the full width at half maximum of the enhancement peaks.

Being a measure of polarization similarity at different spatial locations, the size of the CDMP speckle reflects the extent of the interaction volume necessary for the wave to depolarize, or, in other words, to lose memory of its initial polarization state. In a specific geometry, the

magnitude of this characteristic length scale depends on the number of transport mean free paths [76,77]. Therefore, scattering media characterized by small values of l^* are also expected to generate, at their surface, scattered fields with smaller values for the CDMP speckles. This is exactly what our experiments show; the lowest value of the CDMP speckle corresponds to the strongest scattering in sample D. Remarkably, one single realization of the scattering process is sufficient to provide information similar to that acquired through an ensemble average measurement.

The details of these distributions and the spatial correlation of polarization are tied into the properties and features of the medium. The presence of differently scattering objects either embedded within another scattering medium or sitting at the surface can be detected by observing the polarization similarities. The amount and type of polarization correlations can distinguish between different strengths of scattering, even those that have the same mean strength, i.e. media that scatter light with the same amount of depolarization.

4.1.2 Weak Localization Phenomenon

Specific spatial correlations between sources are capable of producing non-stationary statistics in a scattered field in which the polarization actually has a longer length scale associated with it than intensity. In this context, one intriguing situation is that of the weak localization of waves in reflection [78–81]. When a plane wave is incident upon a random medium, the probabilities of any given scattering path and its time reversed pair are equal, and in the exact backscattering direction, all such pairs interfere constructively. A simple schematic of this can be seen in Figure 4-5a. The location of this maximal interference is independent of a

particular path or realization, leading to a “coherent” effect known as enhanced backscattering (EBS).

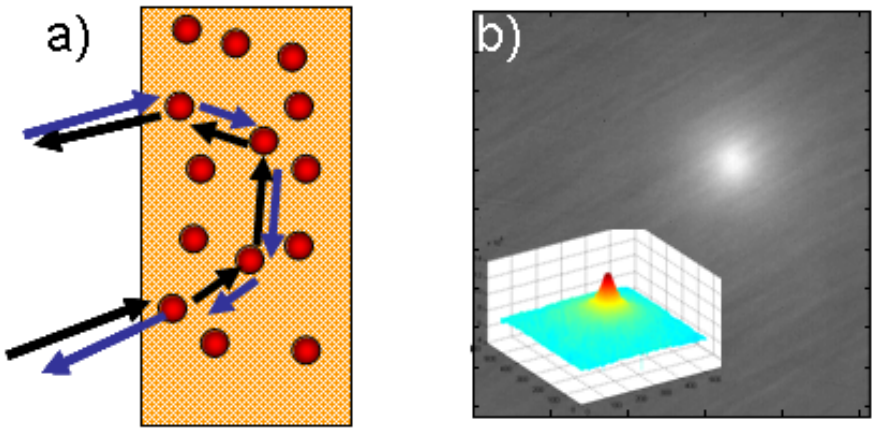

Figure 4-5: (a) Simple schematic of EBS scattering. (b) Ensemble averaged intensity showing the EBS cone and a 3D surface of the relative enhancement (inset).

This enhancement cone manifests itself after ensemble averaging as seen in Figure 4-5b. The maximum theoretical enhancement factor is two times the mean background level [82]. The enhancement cone shape for plane wave illumination follows the relation

$$I(\theta) \propto \mathrm{Re}\left(\int P(\Delta r) exp(ik\theta\Delta r) d(\Delta r)\right), \tag{4.3}$$

where $P(\Delta r)$ is the probability of a photon incident on the surface at a point to emerge at another point separated by some transverse distance Δr. The extent of the angular contributions from the time reversed paths is highly dependent upon the transport mean free path l^* and the angular width $\delta\theta$ is on the order of λ/l^*. As l^* increases, the overall enhancement cone correspondingly decreases [75]. Basically, the incident light probes the medium, and then interferes constructively based upon a material parameter of the medium. From averaged

intensity measurements, the transport mean free path can be estimated from the EBS cone FWHM using the approximation [83]

$$l^* \cong \frac{0.7}{k\theta_{FWHM}(1-R_{eff})}, \tag{4.4}$$

where R_{eff} is the effective reflectance of the interface. EBS is just one phenomenon of light probing media to obtain a mean statistical parameter, such as l^*.

Another interesting aspect of EBS is how the polarization changes across the enhancement peak [80,84,85]. There is a strong dependence on having a similar polarization state such that the time reversed paths can interfere constructively. The intensity of the EBS actually changes from one polarization channel to another as most of the light contributing to the enhancement cone is co-aligned to the polarization state of the incident light [84]. When observed through a cross-polarized analyzer almost of all the light is blocked and only a small resemblance of the enhancement cone is observed, with a severely reduced enhancement factor.

4.1.3 Polarization Similarity in EBS from One Realization

An instance of when the polarization decays on a length scale longer than the intensity occurs in the case of enhanced backscattering [73]. This situation is an excellent example of how examining the polarization fluctuations can reveal more without the need of taking an ensemble average. An ensemble average is the primary method to observe the EBS phenomenon [75]. EBS arises from a situation in which the assumptions of Gaussianity, ergodicity and stationarity are not fully satisfied. When a plane wave is incident upon a random medium, the probabilities of any given scattering path and its time reversed pair are equal. In the exact backscattering direction, all such pairs interfere constructively giving rise to a weak localization,

one that is spatially non-stationary. Of course, in a single realization of wave-matter interaction the presence of an enhancement in the backscattering direction is masked by the random intensity distribution that constitutes the speckle pattern. The existence of this spatial non-stationarity however is present in each realization of the interaction between a coherent wave and a random medium. Since the intensity enhancement relies upon constructive interference, it also implies reliance upon polarization similarity. In the exact backscattering direction, though speckles still occur, these speckles all share a very similar polarization state.

Given a spatial non-stationarity, it follows that the field distribution is non-ergodic. Specifically, as the ensemble average depends on location, it is not possible for the spatial average to equal the ensemble average at every point. However, in practice it may be possible to treat the field as *locally, spatially ergodic*. That is to say that the spatial average over some region about a given point may recover the ensemble average value at that point. However, the concept of local spatial ergodicity raises a number of issues regarding the length scales of the field distribution, the field measurement, and its characterization. For instance, the region of spatial averaging must be sufficiently large to provide reasonable statistics, and yet not so large as to wash out the spatial non-stationarity. We will discuss these aspects in the context of different methods for characterizing such field distributions.

Based on the assumption of local ergodicity over certain spatial domains, we will examine two different methods that may be capable of discerning ensemble-like information from one single realization of the random field. The simplest approach to duplicate the ensemble intensity average is to take a moving spatial intensity average. The effective intensity $\bar{I}$ at a point r calculated for a spatial subdomain A can be defined as

$$\bar{I}_A(r) = \frac{1}{\|A\|}\int_A I(r + r_0)dr_0, \tag{4.5}$$

where

$$I(r) = E_x^*(r)E_x(r) + E_y^*(r)E_y(r). \tag{4.6}$$

As the phenomenon of interference between time reversed paths is polarization dependent, another possibility would be to examine polarimetric quantities [86]. Specifically, the constructive interference relies on polarization similarity, that can be gauged by the degree of polarization estimated over a spatial subdomain A [87]. This the effective degree of polarization $\bar{P}$ as defined by Eq. 4.2. It is interesting to note that, unlike the effective intensity, this quantity inherently involves fourth-order field correlations, and as such, can be expected to be more sensitive to fluctuations in the field distribution [36].

Both parameters defined in Eqs. 4.5 and 4.2 can be used to encode the spatial distribution of a random field (a speckle-like image) by producing an average over a subdomain A and then associating that value with the corresponding location in the initial field. However, the choice for the size of such a subdomain is arbitrary and most importantly, introduces an artificial length scale. In other words, one may find an appropriate size of the subdomain for which the non-stationarity can be revealed but the size of such subdomain is not known a priori; moreover, this choice may depend on characteristic length scales of the specific problem. These length scales are the physical extent of the non-stationarity and the overall size of the available data, i.e. the largest scale length in the random field. In fact, the existence of an appropriate size of the subdomain is inherently tied to the existence of a spatial non-stationarity.

To avoid having to find an optimum size of the subdomain that would reveal a specific non-stationarity, a method similar to that used in LASCA was developed; CDMP calculations of spatial subsets across all the pixels were performed to determine the polarization spatial decay length. As the speckles associated with the time reversed paths have strong polarization similarity, a CDMP analysis was a logical choice. Using the definition in Eq. (2.23), one can calculate the CDMP spatial decay length $\mathcal{L}(r)$ by evaluating in each point r the decay of $\left|V^2(r, r+\delta r)\right|$ for increasing values of δr averaged azimuthally. For identically polarized fields, $\left|V^2(r, r+\delta r)\right|$ is unity, while for a uniformly random distribution of states of polarization $\left|V^2(r, r+\delta r)\right|$ averages to one half. After evaluating the CDMP decay length for each point, these values can be used to generate a completely new spatial representation where each point is encoded in its corresponding value of the CDMP decay length.

All three of these approaches, the effective intensity $\bar{I}$, the effective degree of polarization $\bar{P}$, and the CDMP decay length $\mathcal{L}(r)$ will be used to examine speckle fields that, upon ensemble averaging, manifest coherent backscattering. A single realization of the speckle pattern can be written as

$$I(k_i, k_f) = I_0 + \sum_{l,m} \left|A_{lm}\right|^2 \cos(k_i + k_f) \bullet (r_l - r_m) + F(k_i, k_f), \tag{4.7}$$

where k_i and k_f are the wave vectors of the incident and scattered plane wave and A_{lm} represents the complex amplitude of the wave having r_l and r_m as the ending points of a multiple scattering trajectory inside the random medium [88,89]. The second term in Eq. 4.7 represents the non-stationary component that upon ensemble averaging leads to a cone of enhanced

intensity. This intensity enhancement around the backscattering direction has a width on the order of λ/l^*, where l^* is the so-called transport mean free path. The third term $F(k_i, k_f)$ represents the speckle fluctuations and, in the case of a Gaussian random field, averages to zero.

To test the different methods for locating the presence of non-stationarity, a typical EBS experiment was conducted. The setup, built around a continuous-wave laser operating at 488 nm and a cooled CCD array, was described earlier [90]. In addition, a full polarimetric measurement was performed in each pixel of the resolved speckle using a rotating quarter-wave plate and subsequent Fourier analysis [32]. In the experiments, a 2mm beam was incident on the sample and produced in the plane of the CCD a speckled field with an average size of the speckle of about 64μm. The sample was mounted on a spin plate that allowed observing single realizations of the scattered field as well as the corresponding ensemble average.

The scattering media used were different diffusing materials exhibiting minimal absorption. A large range of transport mean free paths, l^* values, was covered using different solid samples: (A) Suba IV™ polishing pad (Rodel), (B) Spectralon® (Labsphere), (C) Durapore™-HVLP filter paper (Millipore), and (D) compressed TiO2 powder (DuPont). The scattering strengths of these samples are very different. From the widths of the corresponding EBS cones the estimated values of l^* were 40μm, 20μm, and 7μm for samples A, B, and C respectively. For the TiO_2 sample a scattering mean free path of approximately 1μm was determined using optical path-length spectroscopy [59]

The results of applying the analysis methods are summarized in Figure 4-6. The first two rows illustrate a typical realization of the random distribution of backscattered intensity and the corresponding result of the ensemble average, respectively. The familiar appearance of a speckle

field (first row) can be observed for all samples, and as can be seen, no sample specific information is practically available in these intensity distributions.

As a result of the ensemble average on the other hand, the extent of the enhanced intensity may provide means to discriminate between the different structures as can be seen in the second row. However, this ability is restricted by the spatial resolution and the extent of the accessible field (experimentally limited by the pixel size, numerical aperture, and number of pixels available). For instance, in the case of sample D, the ensemble average appears as an almost constant background. It is evident that in this case, one cannot conclude that the absence of a region of enhanced intensity is due to the peak being either too large or too narrow or simply because the recording is performed away from the backscattering direction.

In the third row of Figure 4-6, we present the results of calculating the effective intensity $\bar{I}$ over a region (square box) containing 61 x 61 pixels that was scanned across the entire speckle image shown in the first row. For each location, the value of $\bar{I}$ was attributed to the central pixel of the box. This method basically performs the subset average of intensity including many points instead of the ensemble average at the central point of this domain. Since the average intensity in the EBS region is higher than the background, one could also expect a similar effect in the effective intensity image. However, as can be seen in Figure 4-6, no such increase of intensity can be observed for samples A and D, but the reasons are quite different. In the case A, the non-stationarity cannot be resolved due to the size of the averaging box while in the case D, the process is simply stationary over the limited field available. A certain increased intensity is prevalent in the results for samples B and C where an intensity enhancement concentrated towards the center of the image may indicate the presence of a spatial non-stationarity.

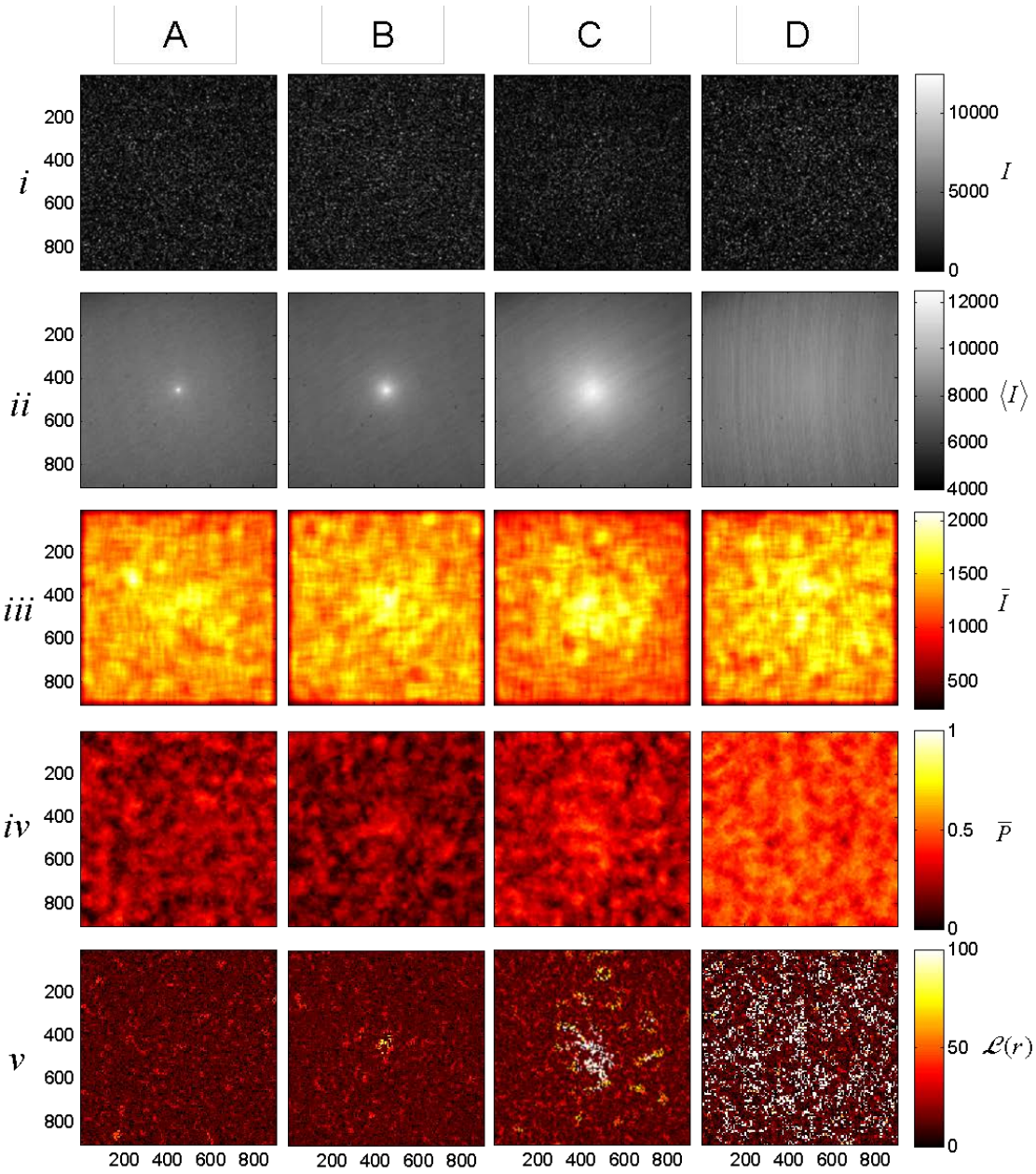

Figure 4-6: Images corresponding to samples A, B, C, and D as described in the text. (i) single realization speckle intensity image, (ii) ensemble average, (iii) image encoded in the calculated effective intensity, (iv) image encoded in the calculated effective degree of polarization, (*v*) image encoded in the calculated polarization decay.

In a completely similar manner, we have evaluated the effective degree of polarization $\bar{P}$ for a circular area with a radius of 31 pixels and the results are shown in the fourth row of Figure

4-6. Because the interference effects leading to the enhanced scattering rely upon polarization similarity, it is expected that regions with a higher degree of polarization should indicate the presence of EBS. This is indeed seen in our results where the $\bar{P}$ values around 0.5 clearly indicate the polarization similarity. It is interesting to note the increase in the $\bar{P}$ values from sample A to D and the existence of non-stationarities similar to the ones in the ensemble averages shown in the second row.

Of course, for a specific sample, both $\bar{I}$ and $\bar{P}$ images could have been optimized in order to illustrate the presence and identify the location of the enhancement peak. However, that would necessitate *a priori* knowledge about the extent of the non-stationarity in order to select an appropriate size of the averaging box as the size of the box is sample specific. This requirement can be avoided by using a higher-order polarimetric measure as demonstrated in the last row of Figure 4-6 where the images are encoded in the decay length of CDMP evaluated as described before. As can be seen, now there is an even stronger progression from left to right. As the size of the enhancement increases, the number of points having longer polarization decay lengths rises. Note that there is no additional image processing involved and that the color coding indicates the actual decay length of CDMP measured in pixels. Samples B, C, and D all show strong spatial polarization correlations with increasing values of the polarization decay lengths. In the case A, there is simply not enough pixel resolution to evaluate a two-point characteristic such as CDMP.

Perhaps the most interesting observation concerns the compressed TiO_2 powder (sample D) which has a very small l^* leading to a large EBS cone. As pointed out before, in this case the ensemble average image cannot confirm the presence of a non-stationarity in the random distribution of intensity. Because of the limited angular resolution of the optical system, one

cannot identify the presence of a region with enhanced intensity. However, the existence of the coherent enhancement is clearly visible in only one realization of the random speckle pattern when the higher-order two-point correlations of the field are examined. The high values of the CDMP decay length clearly indicate the existence of polarization similarities that are specific to EBS. Detailed features of the wave-matter interaction are therefore prevalent in one single realization of the emerging random field but their characterization requires access to higher-order statistics of the field.

4.2 Polarization Length Scales in the Superposition of Random EM Fields

For simplicity, statistical analyses of random optical fields often only involve fields with a single correlation length Λ, in that the average speckle size is constant [91–95]. There can be situations in which the random field under study is actually the superposition of two random fields of different correlation lengths. When this combination is an incoherent superposition, then the two random fields add in intensity and as mentioned in chapter 2, there is a suppression of the intensity fluctuations and the speckle contrast is reduced. A more interesting situation is the coherent superposition of two random fields [96–100]. In this case the two fields add in amplitude, there is no reduction in contrast, and when the two random fields have different correlation lengths, then the two fields interfere constructively creating speckle spots that appear to be speckled themselves. These patterns can otherwise be known as speckled speckle [96].

The occurrence of speckled speckle can often be the norm in experiments due to parasitic scattering, but often the camera resolution is insufficient to resolve the smaller speckle spots. Better knowledge about the occurrence of speckled speckle and the underlying material properties that cause them provides an avenue to learn about the scattering medium from the

statistics of the speckle pattern. In this chapter we present the basis that it may be possible to infer properties of one of the scattered fields with assumptions made on the other. It may be possible to remove the parasitic scattering and examine only the scattering of interest.

4.2.1 Superposition of polarized and unpolarized scattered fields

The statistics of combining two differently polarized speckles fields can further complicate the statistics. An approach is to consider that the resulting random electromagnetic field is the combination of two locally polarized fields: one that is globally unpolarized $\mathcal{U}(r) = E^{\mathcal{U}}(r)\hat{e}(r)$ and the other one characterized by a uniform polarization state, $\mathcal{P}(r) = E^{\mathcal{P}}(r)\hat{e}_0$. The addition of the two quasi-monochromatic and mutually coherent fields leads $E^{\mathcal{R}}(r) = E^{\mathcal{U}}(r)\hat{e}(r) + E^{\mathcal{P}}(r)\hat{e}_0$. As a reminder, the globally unpolarized field is actually the superposition of two uncorrelated orthogonally polarized components, one along *x* and the other one along *y,* for instance. This is the situation described above for the vectorially speckled speckle, but of course the two components in $\mathcal{U}$ are the same correlation length. These two orthogonal fields are added in intensity, reducing the speckle contrast and the further addition of uncorrelated fields would further reduce the contrast. However, when a fully polarized and coherent REF is added to the field $\mathcal{U}$, the optical contrast of $E^{\mathcal{R}}(r)$ actually increases because the uniformly polarized component increases the magnitude of the field amplitude along a certain direction, thus biasing the overall polarization of $E^{\mathcal{R}}(r)$. Not only does the addition of this coherent field increase the contrast, but it also increases the overall degree of polarization creating a partially polarized REF. This is similar to combining a completely unpolarized beam with a fully polarized one to create any partially polarized beam [101,102].

The globally unpolarized field ($\mathcal{U}$) can be modeled as a REF where the complex amplitude components E_x and E_y are both circular Gaussian random functions. Each of these components can be represented as a sum of plane waves

$$E_\mu^{\mathcal{U}}(\mathbf{r}) = \sum_j a_j \exp\left[i\left(k_j \cdot \mathbf{r} + \phi_{\mu,j}\right)\right], \mu = x, y, \tag{4.8}$$

where a_j is an amplitude, k_j are transverse wavenumbers, $\mathbf{r}$ is a position vector, and $\phi_{\mu,j}$ are uniformly random phases. When the field in Eq. (4.8) is added to a field uniformly polarized along *x*,

$$E_x^{\mathcal{P}}(\mathbf{r}) = \sum_j b_j \exp\left[i\left(k_j \cdot \mathbf{r} + \phi_{x,j}\right)\right], \tag{4.9}$$

where b_j is a different set of amplitudes, there are several ways to characterize the properties of the resultant REF. Examples of adding the different underlying speckles is shown in a simple visualization in Figure 4-7 though it is important to note that in reality the fields are added together, not the intensities.

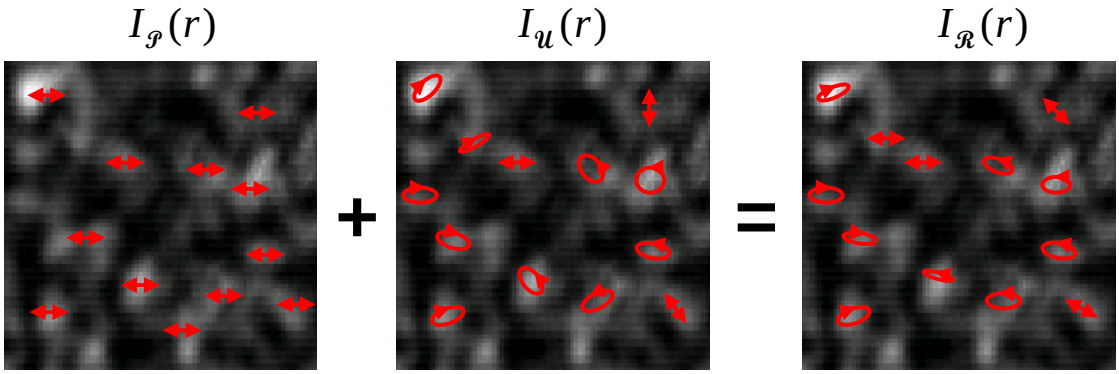

Figure 4-7: Simple visualization of the composition of the underlying field components.

One simple global measure is to compare the average intensity of the field $\mathcal{P}$ with the average intensity in the total field $E^{\mathcal{R}}(r)$. In our practical example, this ratio $\beta = \left\langle \left| E^{\mathcal{P}}(r) \right|^2 \right\rangle / \left\langle \left| E^{\mathcal{R}}(r) \right|^2 \right\rangle$ would indicate the strength of the scattering regime. For instance, for $\beta > 0.5$, the REF would favor the linearly polarized component. We note that this ratio of intensities relates to the global degree of polarization $\bar{P}$ of the final REF. As β continues to increase, $\bar{P}$ increases as well until unity saturation is reached.

Another characteristic of the resultant field is the extent of its field-field correlations. In addition to having different overall magnitudes and polarization characteristics, random fields may also have different field correlation lengths. In other words, the speckle sizes of the fields $\mathcal{U}$ and $\mathcal{P}$ can be different. The short-range correlation length for $\mathcal{U}$ can be defined as

$$\left\langle E^{\mathcal{U}}(\mathbf{r}) E^{\mathcal{U}}(\mathbf{r}+\delta) \right\rangle_{\mathbf{r}} = f(\delta^{\mathcal{U}}), \tag{4.10}$$

and it has the same value for both *x* and *y* field components. The unpolarized field can be caused by any number of strongly scattering media but, for the purpose of this paper, it is assumed that the unpolarized field is examined near its source and, therefore, the field correlation length is of the order of a wavelength [11,13]. The field correlation for the linearly polarized component,

$$\left\langle E_x^{\mathcal{P}}(\mathbf{r}) E_x^{\mathcal{P}}(\mathbf{r}+\delta) \right\rangle_{\mathbf{r}} = f(\delta^{\mathcal{P}}), \tag{4.11}$$

is of course only along *x*. This can result from the scattering from a rough surface, ballistic scattering, and other types of scattering that conserve the state of polarization [7,103]. Along

with the value of β, these two correlation lengths directly influence the length scales of the resulting REF.

As mentioned before, β, $\bar{P}$, and the f factors in Eqs. (4.10) and (4.11) are all global properties, evaluated as ensemble averages. While $\bar{P}$ is indicative of the overlap between the fields $\boldsymbol{\mathcal{U}}$ and $\boldsymbol{\mathcal{P}}$, its value does not take into account the field correlation in the resulting REF. The correlation length on the other hand is a structural characteristic evaluated using a two-point property. As the resulting REF has different levels of partial polarization depending on the strength of $\boldsymbol{\mathcal{P}}$, the polarization structure of the final REF is important to consider.

In section 4.1.1, we demonstrated that a two-point polarization similarity measure such as the complex degree of mutual polarization (CDMP) can conveniently describe the spatial structure of polarization in a REF without requiring an ensemble average [74]. In general, the CDMP factor measures the similarity between two polarization states [40] and it ranges from zero when the two states are orthogonal to unity when the polarization states are identical. For the purpose of the present analysis, the CDMP is defined such that it measures the correspondence between the state of polarization at position r (coordinates x, y) and a chosen reference polarization state:

$$\left|V^2(r)\right| = \frac{\left(E_x^{\mathcal{R}*}(r)E_x^{\mathcal{P}} + E_y^{\mathcal{R}*}(r)E_y^{\mathcal{P}}\right)^2}{\left(\left|E_x^{\mathcal{R}}(r)\right|^2 + \left|E_y^{\mathcal{R}}(r)\right|^2\right)\left(\left|E_x^{\mathcal{P}}\right|^2 + \left|E_y^{\mathcal{P}}\right|^2\right)}. \tag{4.12}$$

In Eq. (4.12), the reference is the polarization state of the field $\boldsymbol{\mathcal{P}}$. Using this definition, one can generate a two-dimensional CDMP map corresponding to this specific state of reference polarization as can be seen in Figure 4-8. This two-dimensional graphical representation of

polarization "speckle" is characterized by spatial features with different sizes and spatial frequencies. Similarly to conventional intensity speckles, it is expected that these features will depend on the properties of $\mathcal{U}$ and $\mathcal{P}$. Of course, since the field $\mathcal{P}$ is in the same polarization state of the reference, its CDMP map would have a uniform value of one; the CDMP map of $\mathcal{U}$ on the other hand should be correlated over distances on the order of $\delta^{\mathcal{U}}$.

As a means to assess the spatial frequencies in these polarization maps, one can examine the power spectral density (PSD) defined as

$$P(\omega) = F\left\{\left|V^2(r)\right| * \left|V^2(r)\right|\right\}, \tag{4.13}$$

where $\left|V^2(r)\right| * \left|V^2(r)\right|$ represents the autocorrelation of a CDMP map. Because the analyzed REF is the superposition of two other fields that are mutually coherent, Eq. (4.13) can be further written as [97]

$$P(\omega) = \bar{I}_1^2 p_1(\omega) + \bar{I}_2^2 p_2(\omega) + \bar{I}_1 \bar{I}_2 p_{12}(\omega) \tag{4.14}$$

where

$$\begin{aligned} p_j(\omega) &= F\left\{a_j^* a_j * a_j^* a_j\right\}, \quad j = 1, 2 \\ p_{12}(\omega) &= F\left\{2a_1^* a_1 * a_2^* a_2 + \left(a_1^* a_2 + a_2^* a_1\right) * \left(a_1^* a_2 + a_2^* a_1\right)\right\} \end{aligned} \tag{4.15}$$

represent the power spectral densities of the individual components and the mixed (interference) term, respectively. In Eq. (4.15), a_1 and a_2 denote the individual, normalized *x* field components $E^{\mathcal{P}}(r)/S_0(r)$ and $E^{\mathcal{U}}(r)/S_0(r)$, respectively. The properties of the spatial distribution of polarization states across a REF relate to the power spectrum of the CDMP map in Eq. (4.13),

which, in our case, depends on the specific values of β and $\delta^{\mathcal{P}}$. Of course, the information content of this power spectrum in Eq. (4.13) is richer than that provided by the value of $\bar{P}$, which is only a global average of point-like properties.

In general, any REF can be decomposed into a globally unpolarized and a uniformly polarized component. These two components have a relative strength β and are also characterized by their, possibly different, coherence lengths $\delta^{\mathcal{U}}$ and $\delta^{\mathcal{P}}$. These characteristics influence the global properties of REF in different ways. For instance, the global degree of polarization $\bar{P}$ of the final REF depends only on the ratio β but is not influenced at all by $\delta^{\mathcal{U}}$ or $\delta^{\mathcal{P}}$. The spatial properties of polarization on the other hand are determined by all these factors as can be seen in the power spectrum of the CDMP map in Eqs. (4.14) and (4.15). Because (i) the global degree of polarization $\bar{P}$ can be determined independently and (ii) the coherence length $\delta^{\mathcal{U}}$ is known to be of the order of the wavelength, one can use the power spectrum of the CDMP map to determine the unknown correlation length $\delta^{\mathcal{P}}$ of the polarized field component. In the following we will illustrate this procedure using systematic numerical simulations.

4.2.2 Numerical simulations of overlapping REF

To illustrate some of the field properties resulting from the superposition of coherent REFs, a simple numerical simulation was performed. Using the plane wave decomposition in Eq. (4.8), plane waves originating from a circular array of source points with random phases were mapped onto an observation plane of 250 by 250 pixels. This creates a Gaussian random field originating from a beam with radius *r*, with a coherence length $\delta^{coh} = 3.83/(\kappa r)$ [7]. When $\kappa = 1$ and $r = 0.3$, the coherence length $\delta^{\mathcal{U}}$ of the globally unpolarized field was set to be equal about

12 pixels in the observation plane. The uniformly polarized field was created in a similar manner using Eq. (4.9) in only one linear state of polarization. In addition, the spatial correlation length of this polarized field ($\delta^{\mathcal{P}}$) was controlled by adjusting the parameter *r* to produce different values that are larger than $\delta^{\mathcal{U}}$. These two random fields are then superposed coherently and the resulting intensity patterns are shown in Figure 4-8 for the case where the coherence length of the polarized field is four times larger than the unpolarized component, i.e. $\delta^{\mathcal{P}} = 4\delta^{\mathcal{U}}$. In this example, the intensity patterns in Figure 4-8a and b are characterized by a ratio $\beta = 0.15$, which corresponds to a global degree of polarization $\bar{P} = 0.11$.

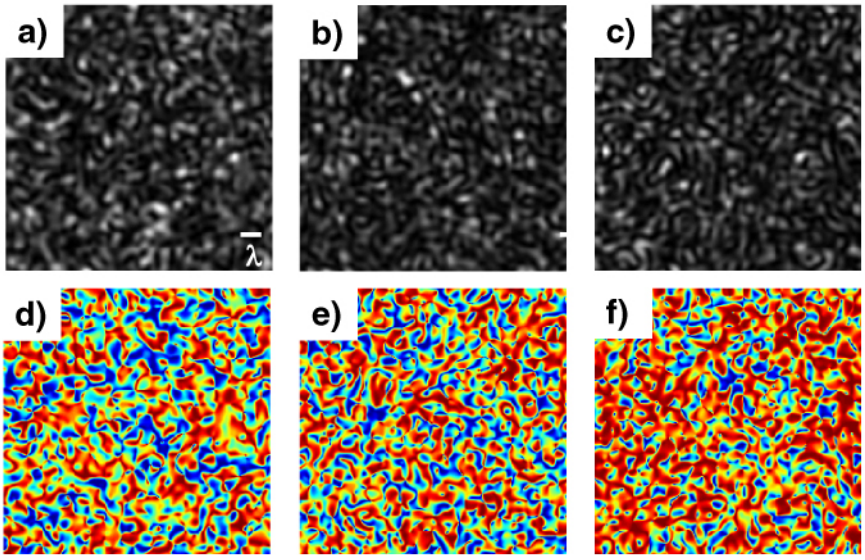

Figure 4-8: Intensity speckle images of the superposition between an unpolarized field of coherence length δ^{U} and a polarized field characterized by: a) $\beta = 0.15$, $\delta^{\mathcal{P}} = 4\delta^{\mathcal{U}}$ b) $\beta = 0.15$, $\delta^{\mathcal{P}} = \delta^{\mathcal{U}}$ c) $\beta = 0.15$, $\delta^{\mathcal{P}} = \delta^{\mathcal{U}}$ and the corresponding CDMP maps for: d) $\beta = 0.15$, $\delta^{\mathcal{P}} = 4\delta^{\mathcal{U}}$ e) $\beta = 0.15$, $\delta^{\mathcal{P}} = \delta^{\mathcal{U}}$ and f) $\beta = 0.45$, $\delta^{\mathcal{P}} = \delta^{\mathcal{U}}$. Areas of blue and red correspond to CDMP values of 0 and 1, respectively. The values of $\beta = 0.15$ and $\beta = 0.45$ correspond to global degrees of polarization $\bar{P} = 0.11$ and $\bar{P} = 0.31$, respectively.

At such a low intensity ratio, adding an additional linearly polarized field has little impact and the resulting REF is almost globally unpolarized. As can be seen, even when the correlation length $\delta^{\mathcal{P}}$ is four times larger than $\delta^{\mathcal{U}}$, there is practically very little change in the size of the final intensity speckles. However, when observing the CDMP maps, one can easily notice changes in the statistical nature of their structure. Even though the two REFs in Figure 4-8a and b have the same global degree of polarization, there is a clear difference in the spatial frequency content of the corresponding CDMP maps as seen by the larger groupings of high CDMP values in Figure 4-8d.

The third speckle pattern in Figure 4-8c corresponds to the situation where $\delta^{\mathcal{P}}$ is equal to $\delta^{\mathcal{U}}$ but the field $\mathcal{P}$ now has a greater amplitude, i.e. the ratio $\beta = 0.45$ and, correspondingly, $\bar{P} = 0.31$. As can be seen, the spatial frequency content in the CDMP map of Figure 4-8f is similar to the one in Figure 4-8e but now with a higher prominence of locations where $\left|V^2(r)\right| = 1$.

To get a quantitative description on how the correlation length of the field $\mathcal{P}$ affects the spatial distribution of polarization in the resulting REF, we have calculated the power spectral density of the CDMP maps resulting from the numerical procedure. An example is illustrated in Figure 4-9 for three cases corresponding to fields $\mathcal{P}$ having different correlation lengths and the same $\beta = 0.45$.

It is clearly seen that the characteristic shape of the curves in Figure 4-9 appears to be composed of three different contributions. This is also described by Eq. (4.14) where the power spectral density contains three main terms that can be approximated by zero-mean Gaussians with different widths. The widths of these Gaussians are representative of the correlation lengths

of the fields $\mathcal{P}$ and $\mathcal{U}$ while their magnitudes depend on the relative strengths of the fields (β). We have also fitted the power spectral densities to the formulation in Eqs. (4.14) and (4.15) using the magnitudes I_1 and I_2 and the three Gaussian widths as fitting parameters. The results are included with continuous lines in Figure 4-9. The first two terms correspond to the power spectral densities of the individual fields $\mathcal{P}$ and $\mathcal{U}$. Since the CDMP maps for the individual fields do not change with β and $\delta^{\mathcal{P}}$, the widths of the first two Gaussians also remain unchanged.

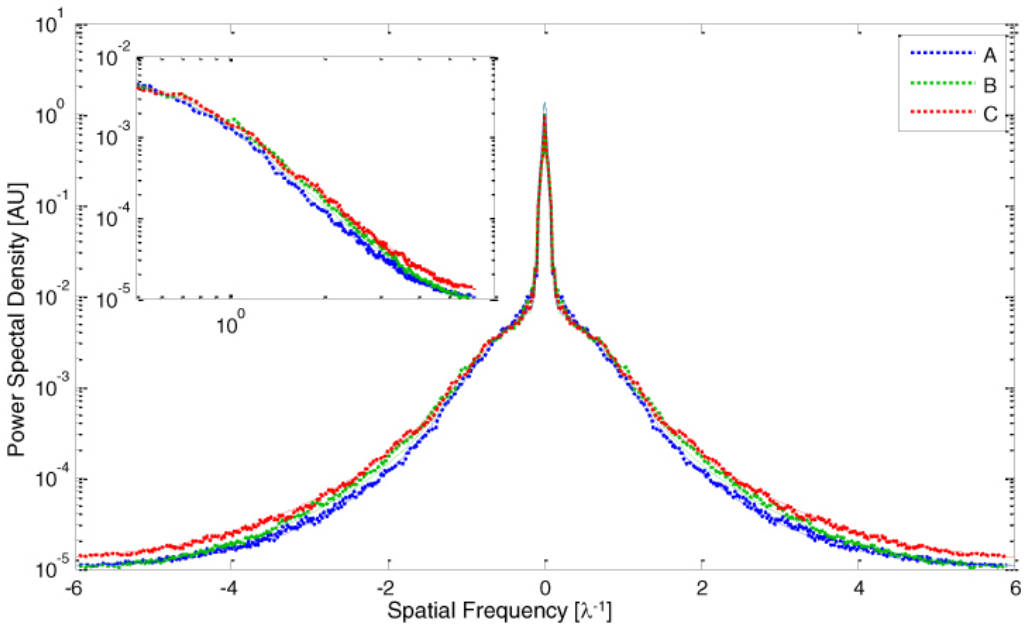

Figure 4-9: The power spectral density of CDMP maps calculated for $\beta = 0.45$ and correlation lengths $\delta^{\mathcal{P}}$ equal to A) $2\delta^{\mathcal{U}}$, B) $4/3\delta^{\mathcal{U}}$, and C) $\delta^{\mathcal{U}}$. Also shown with solid lines are the best fits with power spectrum dependence given in Eq. (4.14). The inset shows a log-log plot of the high spatial frequencies region.

In the specific case analyzed here, the first term, which is basically the PSD of the CDMP map with uniform unity value, has a small Gaussian width of 0.06 in our normalized units (the

narrow central peak in Figure 4-9). The second term represents the PSD corresponding to the unpolarized component and has a constant width of 0.9 due to the fixed correlation length $\delta^{\mathcal{U}}$. The third term in Eq. (4.14) describes the interference between the fields $\boldsymbol{\mathcal{P}}$ and $\boldsymbol{\mathcal{U}}$ with most of its contributions occurring in the high spatial frequency range. In the example presented in Figure 4-9, only the width of this interference term and the magnitudes of the Gaussians depend on the characteristics of the interfering fields. However, because β is constant, all the magnitudes remain unchanged and only the width of the third component changes as $\delta^{\mathcal{P}}$ varies. The contribution of this third term lies mostly in the high frequencies and can be fitted well by a Gaussian function with widths of 3.6, 4, and 5.3 for the PSD labeled A, B, and C, respectively. As can be seen, as the correlation length of $\boldsymbol{\mathcal{P}}$ decreases, the PSD width increases indicating that smaller spatial polarization features appear due to the interference between $\boldsymbol{\mathcal{P}}$ and $\boldsymbol{\mathcal{U}}$.

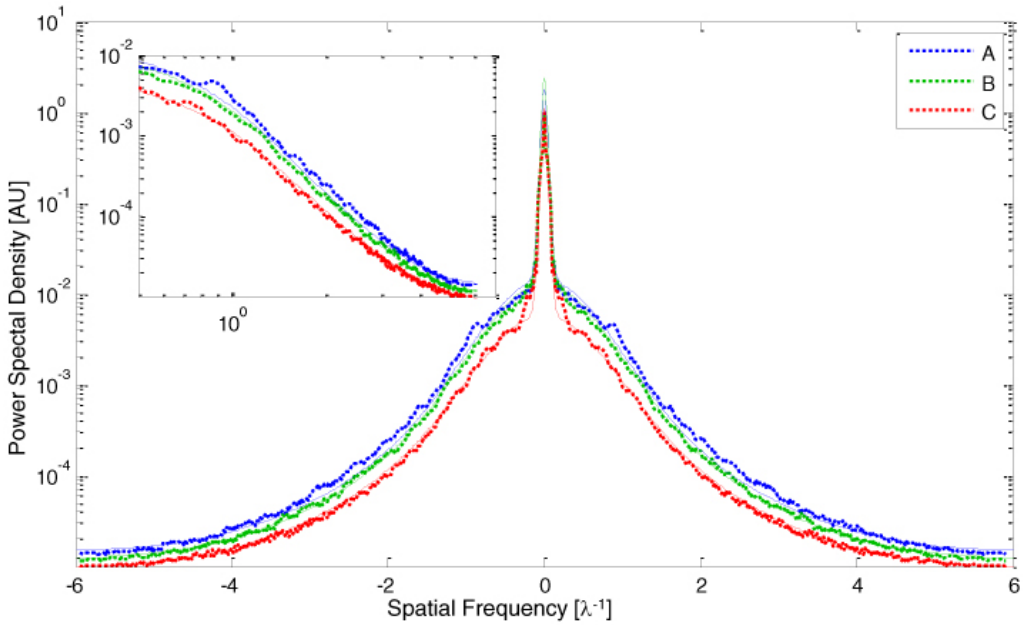

Figure 4-10: The power spectral density of CDMP maps calculated for $\delta^{\mathcal{P}} = 4\delta^{\mathcal{U}}$ and field ratios β equal to A) 0.04, B), 0.19,and C).0.45. Also shown with solid lines are the best fits with power spectrum dependence given in Eq. (4.14). The inset shows a log-log plot of the high spatial frequencies region.

A different example is illustrated in Figure 4-10. Here the correlation length of $\boldsymbol{\mathcal{P}}$ is kept fixed and is four times larger than the field correlation length of $\boldsymbol{\mathcal{U}}$ but the relative strength β is varied. This corresponds to a gradual progression of different polarization regimes. Again, the most interesting features lie in the high spatial frequencies. When fitting the results of the simulation, only the magnitudes of the Gaussians are altered since now the underlying field correlations of the different components are unchanged. As a result, the curves are almost parallel to each other in the high spatial frequency range, as can be clearly seen in the inset. One can also note that, at low β, the influence of the correlation length of field $\boldsymbol{\mathcal{P}}$ is minimal. This is because, when the average strength of the uniformly polarized component increases, the overall content of high spatial frequencies decreases due to a decrease in the magnitude of the second

term in Eq. (4.14). The values of this magnitude are 3.1, 3.0, and 2.6 for the PSDs labeled A, B, and C, respectively. The behavior seen in Figure 4-10 demonstrates that, if the correlations of the underlying fields do not vary during the transition from polarized to globally unpolarized regimes, the shape of the PSD remains relatively unchanged [104].

4.2.3 Autocorrelation of CDMP maps

One way to assess how the combination of the two coherent fields affects the spatial polarization fluctuations is to examine the spatial frequencies and the power spectral density as was shown in the previous section. Alternatively, one can examine directly the distribution of polarization features, i.e. to assess their spatial extent by calculating the autocorrelation of the CDMP map defined as

$$F(x,y) = \left|V^2(m,n)\right| * \left|V^2(m,n)\right| = \iint \left|V^2(m,n)\right|\left|V^2(x+m,y+n)\right| dmdn . \tag{4.16}$$

Note that $F(x,y)$ is a two-dimensional function and its extent represents the average size of the polarization speckle, the region of space where the field's polarization remains essentially the same. As a means to quantify and compare such autocorrelation functions, the second moment is calculated from the cross-section, $F_{CS}(x)$ across the peak of $F(x,y)$

$$\sigma^2 = \sum F_{CS}(x) \cdot x^2 \cdot dx \tag{4.17}$$

where x is the spatial extent of each pixel.

The results of the same numeric simulations described above were analyzed by means of the autocorrelation. An example of autocorrelations of different CDMP maps for varying $\overline{P}$ can be seen in Figure 4-11.

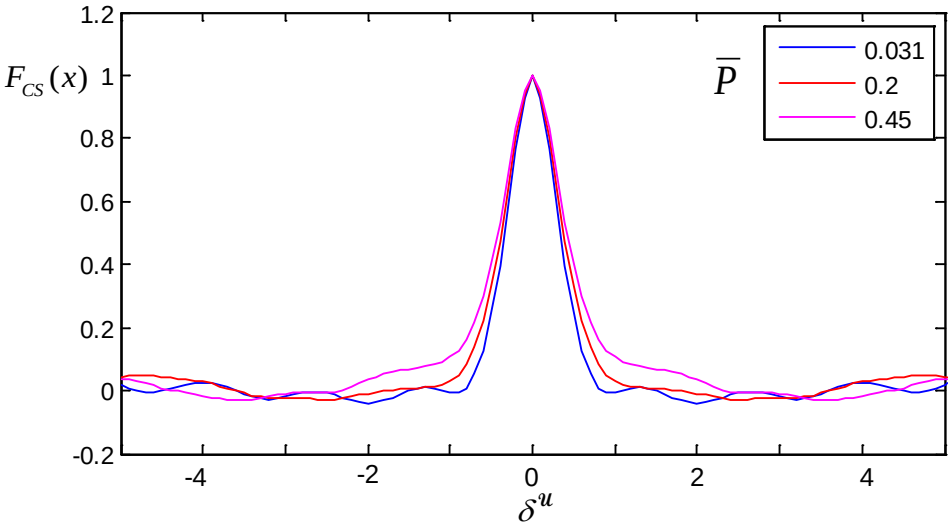

Figure 4-11: Cross-sections through the peak of $F(x,y)$ for equal values of $\delta^{\mathcal{P}}$ and different values of $\overline{P}$.

Just as before when examining the power spectral density, the shape of the CDMP auto-correlation is influenced by the correlation length of the polarized field $\mathcal{P}$ and also by the global degree of polarization $\overline{P}$ of the resultant field. For instance, Figure 4-12 illustrates how the second moment σ^2 of the CDMP auto-correlation increases as $\overline{P}$ increases. Results are presented for different values of $\delta^{\mathcal{P}}$.

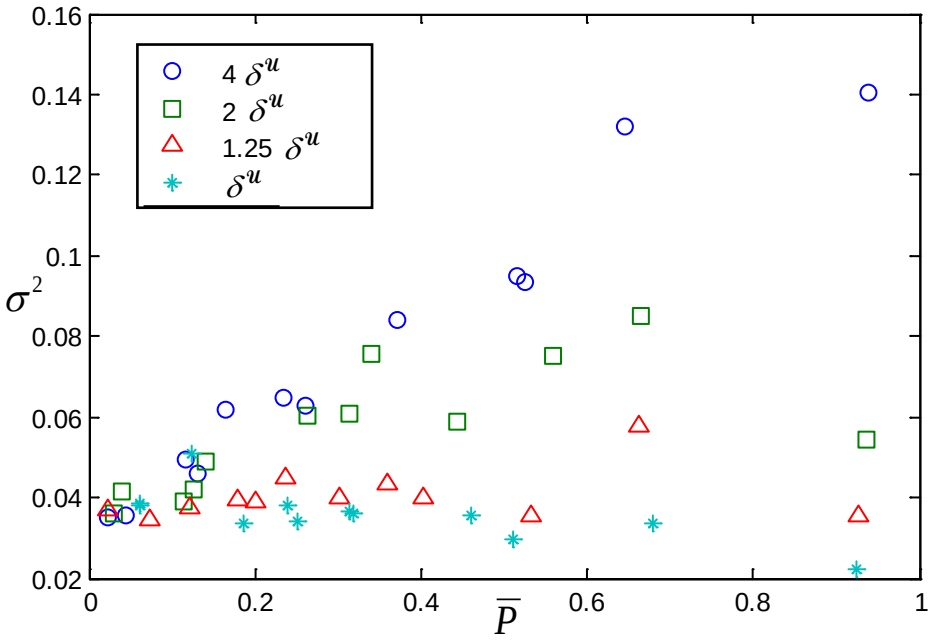

Figure 4-12: 2nd moment of CDMP autocorrelation vs. $\overline{P}$ for correlation lengths $\delta^{\mathcal{P}}$ equal to $4\delta^u$ (blue circles), $2\delta^u$ (green squares), $1.25\delta^u$ (red triangles), and δ^u (light blue stars).

Higher values of σ^2 correspond to a larger spatial extent of the CDMP polarization speckle and, as can be seen, not only does σ^2 increases with $\overline{P}$ but its maximum value also grows when the correlation length of the polarized field $\mathcal{P}$ increases. Since the global degree of polarization $\overline{P}$ is basically the ratio of the two component fields, as $\overline{P}$ approaches one, the uniformly polarized field becomes more dominant. Thus, the corresponding values of σ^2 are larger and the dependence of σ^2 on the degree of polarization is stronger in the case of largest correlation length $4\delta^u$.

Similar results can be observed at a fixed $\overline{P}$ (fixed relative strengths between field components) and increasing the correlation length as shown in Figure 4-13. This figure clearly

demonstrates that when the speckle size associated with the field $\mathcal{P}$ increases, so does the effective CDMP speckle size in the resulting field. We also notice that $\delta^{\mathcal{P}}$ has more impact at higher values of $\bar{P}$ as expected.

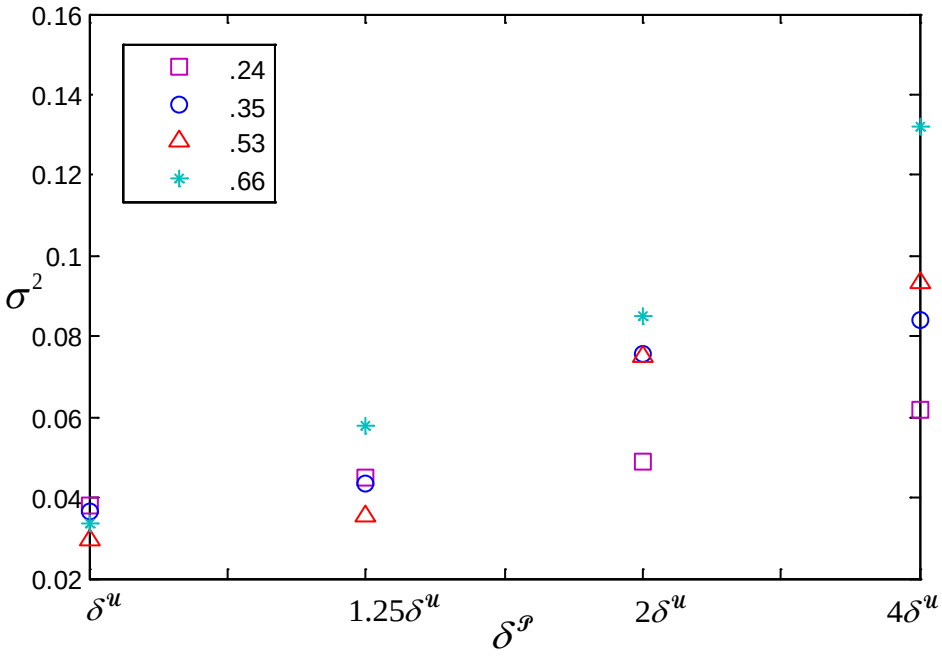

Figure 4-13: 2nd moment of CDMP autocorrelation vs. $\delta^{\mathcal{P}}$ for values $\bar{P}$ of .24 (purple), .35 (blue), .53 (red), and .66 (green).

4.2.4 Experimental analysis of overlapping REFs

All of the above results were calculated from numerical simulations where it was simple to control the two key variables of interfering REFs. To test this model experimentally, the sample scattering medium requires a combination of sources such that the resulting REF measured is a superposition of two underlying REFs. The samples can be a mixture of particle sizes, a bulk scattering medium having a layer of different single scattering particles on the surface or even a varying concentration of suspended particles. It is important to realize that any

dense colloidal suspension can in fact be regarded as a medium generating an unpolarized field corresponding to bulk scattering that is overlapped with a uniformly polarized field corresponding to the single scattering component, originating primarily in the vicinity of the medium's boundary. This observation suggests that the consequences of the model discussed in the preceding section could be relevant for a range of practical situations involving backscattering from random media.

To create this situation experimentally we used a series of colloidal suspensions composed of different particle sizes and having varying concentrations. Increasing the concentration of a colloidal suspension affects its diffusive properties and reduces the transport mean free path l^* of light interacting with it. As the l^* decreases, the strength of scattering increases and one can effectively demonstrate a gradual transition from single to multiple scattering regimes. When a purely single scattering medium is observed in backscattering, the input polarization state is maintained and a uniformly polarized REF results from the light scattered. Speckles are still being created due to the possible phase difference between scattering from different particles situated at different depths. A simple sketch is shown in Figure 4-14. Because sequences containing a large number of scattering events will effectively scramble the initial state of polarization, a purely multiply scattering, fully diffuse medium produces a globally unpolarized REF. In the intermediary situations, the contributions from these two scattering components will mix in different amounts resulting in a partially polarized REF.

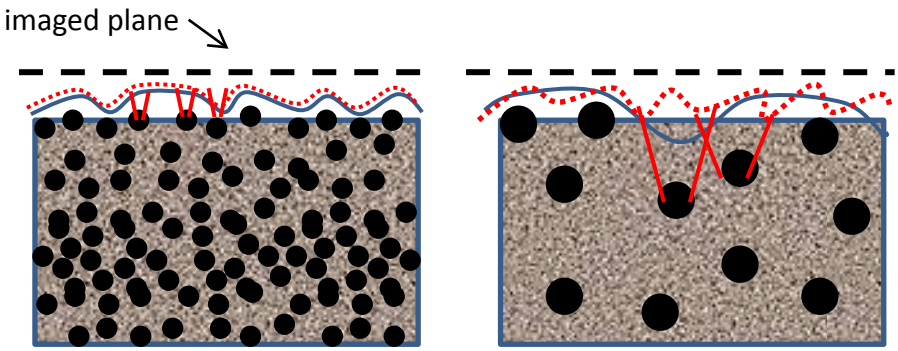

Figure 4-14: Sketch of scattering from colloidal samples with contributions from both bulk and single scattering and similar average properties. The dashed line denotes the effective optical interface and the corresponding REF at this surface.

The samples were prepared by suspending polystyrene spheres in a Laponite® gel which fixes the spheres in place such that there is no movement during measurement and the scattering medium is essentially static. Spheres of sizes 0.33μm, 0.43μm, and 3.7μm were suspended in concentrations such that series of samples having similar values of l^* (60μm, 275μm, 520μm, 1000μm, 2000μm, and 3000μm) were created. The values of l^* were calculated using the Mie scattering cross-section of the particles and the controlled number density of spheres added to the volume.

The samples were placed in a simple imaging setup where they were illuminated with a 488nm argon laser in a backscattering configuration (Figure 4-15). The surface of the sample is imaged onto a CCD after passing through a Fourier Stokes analyzer as described in section 4.1.1. It is important to note that the samples are contained within a cuvette and though the physical surface is flat, the optical surface due to the particles is not necessarily flat as sketched in Figure 4-14. A microscope objective insures the appropriate magnification from the relay lens such that the speckles are fully resolved on the CCD, typically nine pixels per intensity speckle. This

means that the REF mapped onto the CCD is essentially the "close-up" REF that occurs on the sample surface. The CDMP polarization map was then calculated from the Stokes images using the polarization state of the incident beam as the reference and, from these, the auto-correlation and its second moment were calculated.

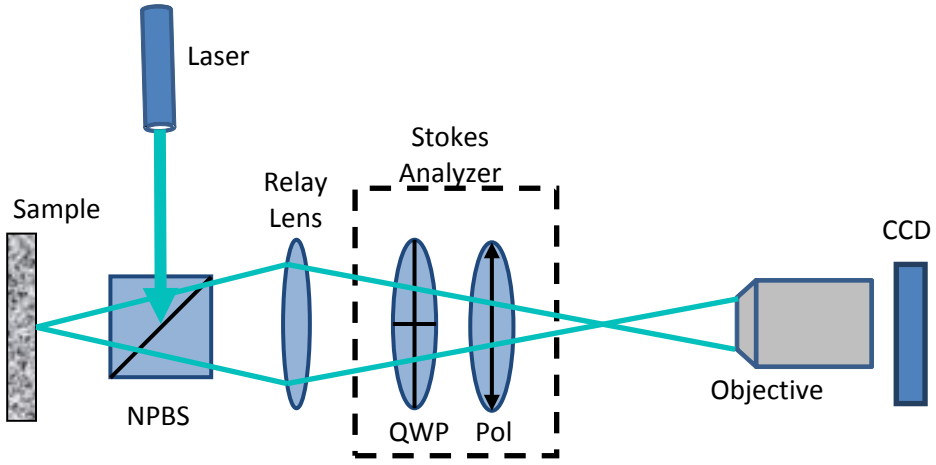

Figure 4-15: Schematic of experimental setup. NPBS – non-polarizing beamsplitter, QWP – quarter wave plate, Pol – polarizer.

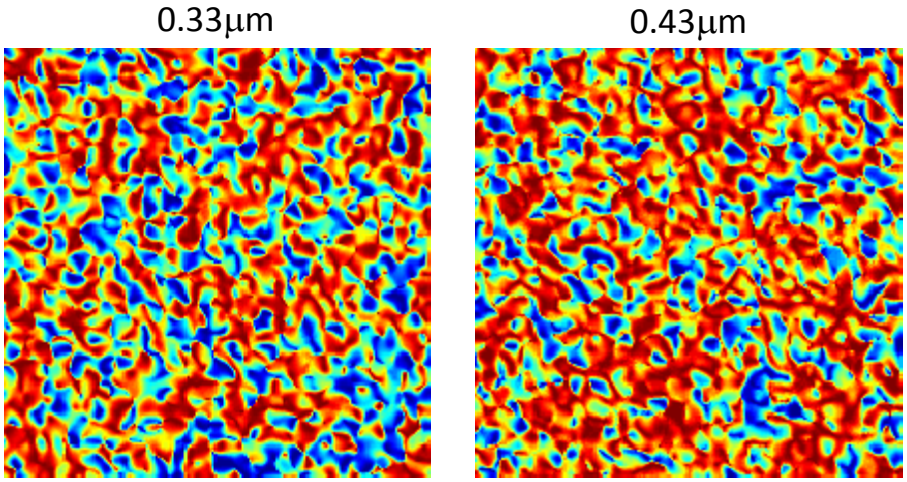

Figure 4-16: CDMP maps resulting from experimental measurements. Results are for particle sizes 0.33μm and 0.43μm at $l^* = 275\mu m$.

Example CDMP maps resulting from the experiment for two particle sizes and equal transport mean free path are shown in Figure 4-16. It can be visually difficult to see many differences between them so the autocorrelations and corresponding 2nd moments were calculated and plotted as presented in Figure 4-17. As can be seen, they follow the general trend observed in the numeric simulations (Figure 4-12). We find that as the value of $\bar{P}$ increases so does the value of the second moment of the autocorrelation of measured CDMP maps. This means that the size of the polarization speckle increases, but more importantly is that the rate of this increase depends on the particle size. This happens because of the differences in the corresponding correlation lengths of the uniformly polarized fields $\mathcal{P}$, which represents the polarization maintaining, single scattering component, specific to each particle size.

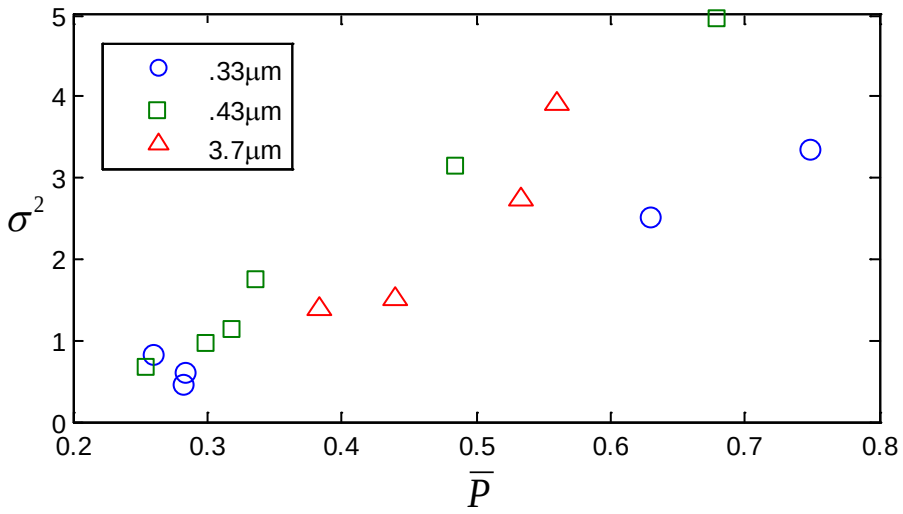

Figure 4-17: Experimental results for σ^2 vs. $\bar{P}$ at particle sizes .33μm (blue circles), .43μm (green squares), and 3.7μm (red triangles).

This difference is clearly observed when examining the spatial extent of the CDMP speckle corresponding to the 0.43μm spheres in comparison to the 0.33μm spheres. The dependence for the 0.43μm has a steeper slope. This can be understood by realizing that the single scattering, uniformly polarized field, corresponding to the larger 0.43μm spheres contributes over larger scattering angles than the slightly smaller 0.33μm spheres. This is somewhat similar with earlier observations that the correlation length of the speckle occurring in the "near-field" from single scattering particles is on the order of the size of the particles themselves [105]. In this reference it was argued that when observing random fields dominated by single scattering, the size of a speckle in the near field is determined only by the spatial extent of the scattering particle [106]. In a transmission geometry, it was found that the speckle size was directly proportional to the particles size and that this value does not depend on the propagation distance z provided that $D^* < D$ [105]. This is an example of how the size of a scattering particle directly influences the correlation lengths associated with the scattered REF.

Although we consider optically dense media in a backscattering geometry, through examining the CDMP we are able to isolate the signature of Mie scattering from particles close to the effective optical surface. By calculating the CDMP with respect to the incident polarization, we essentially isolate the single scattering component of the scattered field in the resulting CDMP polarization map. This means that the larger correlation lengths we observed from the CDMP autocorrelations are due to the larger single scattering angles corresponding to larger particles [107].

Apparently, this simple explanation does not match the experimental measurements on the media containing the much larger spheres of 3.7μm in diameter. In this case we do not

observe an even steeper dependence but instead the polarization length scales lie between those corresponding to previous media, as can be seen in Figure 4-17. The reason for this behavior will be discussed later.

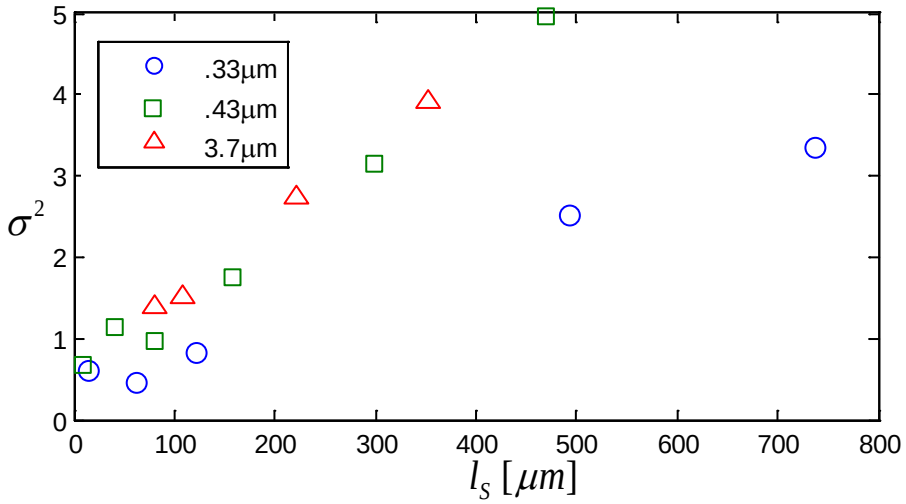

Figure 4-18: Experimental results for σ^2 vs. l_S at particle sizes 0.33μm (blue circles), 0.43μm (green squares), and 3.7μm (red triangles).

Another way to present the data is to examine the second moment variation as a function of the average scattering length l_S as shown in Figure 4-18. Again, these results are very similar to those seen in the simulation and in Figure 4-17. Interestingly, this time, the curve for 3.7μm spheres no longer lies between the other two curves but instead has a slightly steeper slope but, nevertheless, the media comprising the larger 3.7μm spheres behave differently than the others. Let us examine the underlying scattering from these samples more carefully. Whereas the 0.43μm and 0.33μm scattering samples are very similar in size, the 3.7μm spheres are one order of magnitude larger and, therefore, the packing of the spheres is inherently different to insure similar overall optical properties. Due to the large size of the spheres, a fewer number of spheres

is required to achieve similar average scattering lengths and this results in a lower concentration and, consequently, much larger separations between the individual spheres. Within the range of l_S values between 40μm and 200μm, the smaller particles had an average separation of 2μm to 3μm between them. When compared over a similar range of l_S, the 3.7μm particles had average separation distances ranging from 11μm to 18μm. This is a significant difference as it creates a very rough effective optical interface. In other words, particles situated at a range of depths of tens of wavelengths will contribute to the field in the imaging plane.

Since the calculation of CDMP effectively removes the influences from the bulk scattering and exposes the single scattering contributions it's important to know how the single scattering is produced. Smaller particles are relatively closely packed together and scattering from individual spheres occurs effectively in the same imaging plane producing a polarized REF with properties as described in Figure 4-14, i.e. having the correlation length proportional to scatter's size.

As a result, the polarized scattering component is no longer representative solely to single scattering events from individual spheres. The polarized component in the imaging plane is now the interference of contributions originating at different depths. As a result the characteristic lengths scales in this additional interference pattern are smaller and no longer representative for the size of the backscattering particles. The stronger optical roughness for the 3.7μm particles adds additional fragmentation to its component field $\mathcal{P}$ which leads to a smaller correlation length than expected as seen in Figure 4-17 and Figure 4-18. The larger particles also affect the overall global degree of polarization differently. Figure 4-19 shows that for equivalent l_S, the 3.7μm particles tend to maintain the incident polarization state better resulting in a higher $\bar{P}$.

This is the reason why, not realizing the differences between the optical situations, one could perhaps interpret the experimental observations in terms of a smaller particle size. In is important to consider all characteristics and a values available as we have shown with different plots of different properties. In spite of the disagreement in expected results for the much larger particles, we've shown that we've been able to effectively discriminate the relative sizes of the similar scattering spheres.

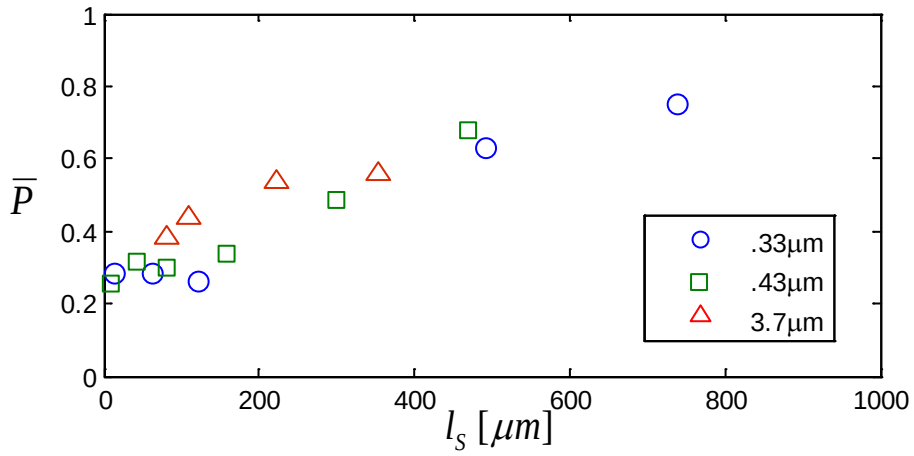

Figure 4-19: Experimental results for $\overline{P}$ vs. l_S at particle sizes 0.33μm (blue circles), 0.43μm (green squares), and 3.7μm (red triangles)

4.3 Summary

The results in this chapter demonstrate that for media with similar diffusive properties in average it is still possible to identify the size of an effective scatter. We examined the practically relevant geometry of backscattering and found that the single scattering contribution largely retains the information about the state of polarization of the incident field. Thus, the single scattering component is primarily polarized uniformly and its contribution to the total REF could

be isolated through a careful polarization analysis. Calculating and examining the spatial extent of the CDMP speckle provides direct insight into the spatial properties of the uniformly polarized scattering component, which is primarily caused by single scattering.

It is interesting to point out that this polarization analysis allowed us to discern the relative sizes of individual scatterers in media that have very similar average properties. Our simple model that described the formation of the single scattering component recovers the main features of the polarized field as long as the characteristics of individual scatterers are not very different from each other. In the case of significantly greater particle size, the inherent larger spacing between the particles requires more advanced modeling involving a description of the actual location of particles. Finally, it should be emphasized again that all the information recovered is the result of a single realization of the light-matter interaction.

There are many practical situations when the emerging random electromagnetic fields can be thought as a combination of two interfering mutually coherent fields. When one of these two underlying fields is globally unpolarized and the other one is polarized uniformly, the spatial correlation of the polarization states contains information about both the relative strength and the extent of the field correlations in the two components.

We have shown that the complex degree of polarization (CDMP), a two-point vectorial descriptor quantifying the polarization similarities in the resulting random field, can be used to recover a wealth of information. In addition to being able to extract a relative particle size from an optically dense colloidal suspension, it can be used to identify non-stationarities that are typically only observed in the ensemble average such as the weak localization phenomenon. Having access to polarimetric information across the spatial extent of the field allows building fourth-order joint statistical parameters. Furthermore, when using mutual polarization measures

such as the CDMP decay length these features can be found without any prior knowledge of the spatial size of the non-stationarity. We have shown that fourth-order field correlations evaluated at pairs of points in a random electromagnetic field can reveal properties that until now were inferred only through an ensemble average.

It is also important to note that all results presented within this chapter are from a single realization of light matter interaction. Without the need for an ensemble average, this coherent assessment of light scattering may become relevant for the study of ultrafast and transient phenomena or in situations that require a large number of realizations such as the search for Anderson localization [108]. On the other hand, very slow processes that are essentially stationary in time may be characterized for one single realization of the scattering medium. Overall, it is important to fully analyze each and every realization of scattering incident to extract all available information.

CHAPTER 5: CONCLUSIONS AND SUMMARY OF ORIGINAL CONTRIBUTIONS

As most sensing scenarios of interest involve realistic random fields, stochastic approaches have the potential to provide fundamentally new functionalities. Some of the approaches to solve specific inverse problems described within this dissertation rely on various modalities to perform a large number of target interrogations. Sometimes however this may not be possible and the work described within this dissertation addresses the question: can this interrogation be done in a parallel manner such that “instantaneous" measurements can be performed? Or, alternatively, how much information can be recovered when one has access only to a limited number of statistical realizations of light-matter interaction?

When waves interact with a random medium, each particular realization of disorder has its own pattern of fluctuations in the scattered wave. It was shown in Chapter 2 that often the intensity fluctuations have universal statistical properties, independent of the scattering medium. Yet, there are also instances where the scattering medium does not exhibit universal properties, and especially when considering the vectorial fluctuations these non-universal properties provide additional insight to the light-matter interaction. Chapter 2 highlighted a few situations in which non-Gaussian unpolarized fields have different statistical properties. This was demonstrated by examining the scattered optical fields from particles of different shapes and calculating higher order correlations of polarization Stokes vector elements.

It has been shown that the interaction of light and matter is a non-self-averaging process, and the complicated features of the scattered waves are all rooted in the structural properties of the specific realization of randomness [11,81,109]. Chapter 3 highlighted some typical

approaches to solving an inverse problem that involve averaging over an ensemble of disorder realizations to achieve mean statistical properties. Unfortunately, this averaging inherently discards information specific to particular realizations as well as the variations from one realization to the next. It is possible though, when examining the fluctuations of scattered waves resulting from the interaction between coherent fields and disordered media. We have demonstrated that analyzing individual members of the ensemble of interactions provides means to extract information beyond that available in the ensemble average. As shown in the case of OPS, The deviation of an individual path-length distribution from the ensemble average is a non-stationary random process which also varies from one realization to another. We have shown that specific properties of the random medium's morphology can be evidentiated by using the scale dependent entropy associated with the variance of path-length fluctuations [64].

There can also be other situations in which examining the fluctuations of REFs is essential especially when performing an ensemble average is difficult due to temporal limitations. In other situations, physical phenomena simply do not permit constructing an ensemble average (a random process that occurs only for a limited period of time for example). This makes it all the more important to measure spatially resolved REFs when possible and examine the vectorial fluctuations. By means of examining higher order correlations and the CDMP of REFs, we have found that the spatial variability of the vectorial properties can be markedly different even when the random fields have similar global properties [74]. We showed that the point and point-pair correlations of the complex degree of mutual polarization provide means to identify the origins of scattered fields of different strengths and demonstrated that the extent of these spatial correlations is determined by the magnitude of the transport mean free path characterizing the scattering process. Spatially resolved measurements of the polarization

properties in one realization of the scattered field allow recovering information otherwise available only through ensemble averages.

A number of applications could benefit from a proposed non-traditional sensing approach including techniques that require fast “one-shot" interrogations or measurements on non-stationary, excitation-induced processes. If the properties of the randomly inhomogeneous medium vary in time then the speckle pattern is dynamic and similar assumptions are usually made about the temporal stationarity and ergodicity. However, there are instances in which the assumptions of Gaussianity, stationarity, and ergodicity are not fully satisfied, for instance EBS. Based on evaluating high-order field correlations (CDMP) in one single realization of the random field, we have been able to demonstrate the presence of source correlation induced non-stationarities [73].

The topic of solving complex inverse problems of wave-matter interaction is of increasing interest especially within the scope of detecting embedded objects or in the context of waves propagating in highly scattering media. Of particular importance is examining the sources of REFs from one single realization, especially when REFs are interfering as explored in Chapter 4. There are different physical situations that lead to interfering random fields. For instance, different random phase screens in the arms of an interferometer, the boundary of two different scattering media, or perhaps the conglomeration of two different types of scattering particles each of which is associated with a different correlation length in its scattered electromagnetic field.

It is also possible to consider random media of different scattering strengths as being the superposition of a globally unpolarized field resulting from the bulk and a uniformly polarized field resulting from single scattering from the particles, especially on the surface. The spatial

correlation of the polarization states or a REF resulting from a single realization contains information about both the relative strength and the extent of the field correlations in the two components [104]. The spatial extent of the CDMP speckle varies and depends on the underlying properties of the single scattering field such as the size of a typical scatterer. The CDMP maps corresponding to media of equal scattering strength but different particles sizes reveal the different REF correlation lengths associated with the particle size [107]. The strategies described here lay the ground work to expand this to situations of more practical interest, i.e. regimes defined by stronger multiple scattering contributions. In such cases multiple scattering introduces too much complication to the observed speckle pattern, but using the appropriate higher-order correlations, and considering the vectorial nature of the random electromagnetic fields, the correlation length due to multiple scattering can be removed and the correlation length of the singly scattered fields can be discerned.

Notably, this information can be obtained from one single realizations of the light-matter interaction. In remote sensing or detection, understanding properties of the target medium or even the scattering properties of the propagation medium is of great importance. There are many methods and solutions attempting to solve the complex inverse problem of wave-matter interaction. The ability to detect or discern material characteristics from a single realization is of great interest, especially in single event situations or when an ensemble is not feasible. Higher order correlations and analyses taking advantage of the polarization correlations of REFs such as those outlined in this dissertation provide the means to further describe the complex scattering nature of random media.

APPENDIX

PUBLICATIONS AND PRESENTATIONS

Publications

1. J. Broky, A. Dogariu, “Polarization correlations in backscattering from media with different optical densities,” (In Preparation).

2. J. Broky, A. Dogariu, “Correlations of polarization in random electro-magnetic fields” Opt. Express 19, 15711-15719 (2011).

3. J. Broky, A Dogariu, “Complex degree of mutual polarization in randomly scattered fields,” Opt. Express **18**, 20105-20113 (2010).

4. J. Broky, K. M. Douglass, J. Ellis, A. Dogariu, “Fluctuations of scattered waves: going beyond the ensemble average,” Opt. Express **17,** 10466-10471 (2009).

5. G. A. Siviloglou, J. Broky, A. Dogariu, and D. N. Christodoulides, “Airy beams: a new class of optical waves,” Opt Photonics News **19**, 21 (2008).

6. J. Broky, J. Ellis, and A. Dogariu, “Identifying non-stationarities in random EM fields: are speckles really disturbing?,” Opt. Express **16**, 14469-14475 (2008).

7. J. Broky, G. A. Siviloglou, A. Dogariu, and D. N. Christodoulides, “Self-healing properties of optical Airy beams,” Opt. Express **16**, 12880-12891 (2008).

8. G. A. Siviloglou, J. Broky, A. Dogariu, and D. N. Christodoulides, “Ballistic dynamics of Airy beams,” Opt. Lett. **33**, 207-209 (2008).

9. G. A. Siviloglou, J. Broky, A. Dogariu, and D. N. Christodoulides, “Observation of accelerating Airy beams,” Phys. Rev. Lett. **99**, 213901 (2007).

Oral Presentations

1. J. Broky and A. Dogariu, “Correlations of Polarization in Random Electromagnetic Fields,” in *Frontiers in Optics* (2011), FWX3

2. G. A. Siviloglou, J. Broky, A. Dogariu, and D. N. Christodoulides, "Observation of Accelerating Airy Beam Ballistics," in *Quantum Electronics and Laser Science Conference* (2008), QTuI4.

3. J. Broky, J. Ellis, and A. Dogariu, "Identifying Non-Stationarities in Random EM Fields: Are Speckles Really Disturbing?," in *Frontiers in Optics* (2008), FThT8.

4. G. A. Siviloglou, J. Broky, A. Dogariu, and D. N. Christodoulides, "Self-Healing of Optical Airy Beams," in *Frontiers in Optics* (2008), FThU6.

5. J. Broky, J. Ellis, K. Douglass, and A. Dogariu, "Statistical Fluctuations: Going Beyond the Ensemble Average," in *Frontiers in Optics* (2008), FWV5.

6. J. Broky, J. Ellis, and A. Dogariu, "Polarimetric Filtering of Time-Reversal in Multiple Scattering," in *Frontiers in Optics* (2007), FTuH5.

7. J. Broky, G. Siviloglou, A. Dogariu, and D. Christodoulides, "Observation of Accelerating Airy Beams," in *Frontiers in Optics* (2007), PDP_B3.

8. J. Ellis, J. Broky, and A. Dogariu, “Polarization Correlations and Speckle Statistics”, SPIE Annual Meeting (2005).

LIST OF REFERENCES

1. A. Ishimaru, *Wave Propagation and Scattering in Random Media* (John Wiley and Sons, 1999).

2. S. Feng, C. Kane, P. A. Lee, and A. D. Stone, "Correlations and Fluctuations of Coherent Wave Transmission through Disordered Media," Phys. Rev. Lett. **61**, 834–837 (1988).

3. P. A. Lee and A. D. Stone, "Universal Conductance Fluctuations in Metals," Phys. Rev. Lett. **55**, 1622–1625 (1985).

4. J. C. Dainty, *Laser Speckle and Related Phenomena* (Springer-Verlag, 1984).

5. M. C. W. van Rossum and T. M. Nieuwenhuizen, "Multiple scattering of classical waves: microscopy, mesoscopy, and diffusion," Rev. Mod. Phys. **71**, 313–371 (1999).

6. J. W. Goodman, "Some fundamental properties of speckle," J. Opt. Soc. Am. **66**, 1145–1150 (1976).

7. J. W. Goodman, *Speckle Phenomena in Optics: Theory and Applications* (Roberts and Company Publishers, 2007).

8. A. H. Gandjbakhche and G. H. Weiss, "V: Random Walk and Diffusion-Like Models of Photon Migration in Turbid Media," in *Progress in Optics* (Elsevier, 1995), Vol. Volume 34, pp. 333–402.

9. J. W. Goodman, "Probability density function of the sum of N partially correlated speckle patterns," Optics Communications **13**, 244–247 (1975).

10. R. Berkovits and S. Feng, "Correlations in coherent multiple scattering," Physics Reports **238**, 135–172 (1994).

11. B. Shapiro, "Large Intensity Fluctuations for Wave Propagation in Random Media," Phys. Rev. Lett. **57**, 2168–2171 (1986).

12. I. Freund, M. Rosenbluh, and S. Feng, "Memory Effects in Propagation of Optical Waves through Disordered Media," Phys. Rev. Lett. **61**, 2328–2331 (1988).

13. M. J. Stephen and G. Cwilich, "Intensity correlation functions and fluctuations in light scattered from a random medium," Phys. Rev. Lett. **59**, 285–287 (1987).

14. A. Z. Genack and N. Garcia, "Intensity Statistics and Correlation in Absorbing Random Media," Europhysics Letters (EPL) **21**, 753–758 (1993).

15. M. P. van Albada, J. F. de Boer, and A. Lagendijk, "Observation of long-range intensity correlation in the transport of coherent light through a random medium," Phys. Rev. Lett. **64**, 2787–2790 (1990).

16. M. C. W. van Rossum, J. F. de Boer, and T. M. Nieuwenhuizen, "Third cumulant of the total transmission of diffuse waves," Phys. Rev. E **52**, 2053–2065 (1995).

17. C. P. Umbach, S. Washburn, R. B. Laibowitz, and R. A. Webb, "Magnetoresistance of small, quasi-one-dimensional, normal-metal rings and lines," Phys. Rev. B **30**, 4048–4051 (1984).

18. M. Stoytchev and A. Z. Genack, "Measurement of the Probability Distribution of Total Transmission in Random Waveguides," Phys. Rev. Lett. **79**, 309–312 (1997).

19. P. A. Lee, A. D. Stone, and H. Fukuyama, "Universal conductance fluctuations in metals: Effects of finite temperature, interactions, and magnetic field," Phys. Rev. B **35**, 1039–1070 (1987).

20. I. Freund, M. Kaveh, R. Berkovits, and M. Rosenbluh, "Universal polarization correlations and microstatistics of optical waves in random media," Phys. Rev. B **42**, 2613–2616 (1990).

21. L. Wang, T. Tschudi, T. Halldórsson, and P. R. Pétursson, "Speckle Reduction in Laser Projection Systems by Diffractive Optical Elements," Appl. Opt. **37**, 1770–1775 (1998).

22. J. G. Manni and J. W. Goodman, "Versatile method for achieving 1% speckle contrast in large-venue laser projection displays using a stationary multimode optical fiber," Opt. Express **20**, 11288–11315 (2012).

23. B. Redding, M. A. Choma, and H. Cao, "Spatial coherence of random laser emission," Opt. Lett. **36**, 3404–3406 (2011).

24. B. Redding, M. A. Choma, and H. Cao, "Speckle-free laser imaging using random laser illumination," Nature Photonics **6**, 355–359 (2012).

25. E. Akkermans, P. E. Wolf, R. Maynard, and G. Maret, "Theoretical study of the coherent backscattering of light by disordered media," Journal de Physique **49**, 22 (1988).

26. M. P. van Albada and A. Lagendijk, "Vector character of light in weak localization: Spatial anisotropy in coherent backscattering from a random medium," Phys. Rev. B **36**, 2353–2356 (1987).

27. I. Freund, "Optical intensity fluctuations in multiply scattering media," Optics Communications **81**, 251–258 (1991).

28. I. Freund, "Stokes-vector reconstruction," Opt. Lett. **15**, 1425–1427 (1990).

29. I. Freund, "Image reconstruction through multiple scattering media," Optics Communications **86**, 216–227 (1991).

30. S. M. Cohen, D. Eliyahu, I. Freund, and M. Kaveh, "Vector statistics of multiply scattered waves in random systems," Phys. Rev. A **43**, 5748–5751 (1991).

31. J. Hurwitz, "The Statistical Properties of Unpolarized Light," J. Opt. Soc. Am. **35**, 525–531 (1945).

32. E. Collett, *Polarized Light: Fundamentals and Applications*, 1st ed. (CRC Press, 1992).

33. J. Ohtsubo and T. Asakura, "Measurement of surface roughness properties using speckle patterns with non-gaussian statistics," Optics Communications **25**, 315–319 (1978).

34. E. Jakeman, "Polarization characteristics of non-Gaussian scattering by small particles," Waves in Random Media **5**, 427–442 (1995).

35. J. Ellis and A. Dogariu, "Differentiation of globally unpolarized complex random fields," J. Opt. Soc. Am. A **21**, 988–993 (2004).

36. J. Ellis and A. Dogariu, "Discrimination of globally unpolarized fields through Stokes vector element correlations," J. Opt. Soc. Am. A **22**, 491–496 (2005).

37. F. Gori, "Matrix treatment for partially polarized, partially coherent beams," Opt. Lett. **23**, 241–243 (1998).

38. E. Wolf, "Unified theory of coherence and polarization of random electromagnetic beams," Physics Letters A **312**, 263–267 (2003).

39. J. M. Movilla, G. Piquero, R. Martínez-Herrero, and P. M. Mejías, "Parametric characterization of non-uniformly polarized beams," Optics Communications **149**, 230–234 (1998).

40. J. Ellis and A. Dogariu, "Complex degree of mutual polarization," Opt. Lett. **29**, 536–538 (2004).

41. M. Draijer, E. Hondebrink, T. Leeuwen, and W. Steenbergen, "Review of laser speckle contrast techniques for visualizing tissue perfusion," Lasers in Medical Science **24**, 639–651 (2008).

42. J. D. Briers and S. Webster, "Laser speckle contrast analysis (LASCA): a nonscanning, full-field technique for monitoring capillary blood flow," Journal of Biomedical Optics **1**, 174–179 (1996).

43. J. D. Briers and G. J. Richards, "Laser speckle contrast analysis (LASCA) for flow measurement," Society of Photo-Optical Instrumentation Engineers (SPIE) Conference Series **3098**, 211–221 (1997).

44. J. D. Briers, "Laser speckle contrast imaging for measuring blood flow," Optica Applicata **37**, 139 (2007).

45. S. Yuan, A. Devor, D. A. Boas, and A. K. Dunn, "Determination of optimal exposure time for imaging of blood flow changes with laser speckle contrast imaging," Appl. Opt. **44**, 1823–1830 (2005).

46. J. D. Briers and S. Webster, "Quasi real-time digital version of single-exposure speckle photography for full-field monitoring of velocity or flow fields," Optics Communications **116**, 36–42 (1995).

47. A. F. Fercher and J. D. Briers, "Flow visualization by means of single-exposure speckle photography," Optics Communications **37**, 326–330 (1981).

48. E. Archbold and A. E. Ennos, "Displacement Measurement from Double-exposure Laser Photographs," Optica Acta: International Journal of Optics **19**, 253–271 (1972).

49. K. Iwata, T. Hakoshima, and R. Nagata, "Measurement of flow velocity distribution by multiple-exposure speckle photography," Optics Communications **25**, 311–314 (1978).

50. D. A. Boas and A. K. Dunn, "Laser speckle contrast imaging in biomedical optics," Journal of Biomedical Optics **15**, 011109–011109–12 (2010).

51. J. D. Briers, G. Richards, and X. W. He, "Capillary Blood Flow Monitoring Using Laser Speckle Contrast Analysis (LASCA)," Journal of Biomedical Optics **4**, 164–175 (1999).

52. H. Cheng, Q. Luo, S. Zeng, S. Chen, J. Cen, and H. Gong, "Modified laser speckle imaging method with improved spatial resolution," Journal of Biomedical Optics **8**, 559–564 (2003).

53. B. J. Berne and R. Pecora, *Dynamic Light Scattering: With Applications to Chemistry, Biology, and Physics* (Courier Dover Publications, 2000).

54. G. Maret and P. E. Wolf, "Multiple light scattering from disordered media. The effect of brownian motion of scatterers," Zeitschrift für Physik B Condensed Matter **65**, 409–413 (1987).

55. D. J. Pine, D. A. Weitz, P. M. Chaikin, and E. Herbolzheimer, "Diffusing wave spectroscopy," Phys. Rev. Lett. **60**, 1134–1137 (1988).

56. P. D. Kaplan, A. G. Yodh, and D. J. Pine, "Diffusion and structure in dense binary suspensions," Phys. Rev. Lett. **68**, 393–396 (1992).

57. D. A. Boas, L. E. Campbell, and A. G. Yodh, "Scattering and Imaging with Diffusing Temporal Field Correlations," Phys. Rev. Lett. **75**, 1855–1858 (1995).

58. R. Carminati, R. Elaloufi, and J.-J. Greffet, "Beyond the Diffusing-Wave Spectroscopy Model for the Temporal Fluctuations of Scattered Light," Phys. Rev. Lett. **92**, 213903 (2004).

59. G. Popescu and A. Dogariu, "Optical path-length spectroscopy of wave propagation in random media," Opt. Lett. **24**, 442–444 (1999).

60. G. Popescu and A. Dogariu, "Scattering of low coherence radiation and applications," The European Physical Journal- Applied Physics **32**, 73–93 (2005).

61. R. C. Youngquist, S. Carr, and D. E. N. Davies, "Optical coherence-domain reflectometry: a new optical evaluation technique," Opt. Lett. **12**, 158–160 (1987).

62. D. A. Boas, K. K. Bizheva, and A. M. Siegel, "Using dynamic low-coherence interferometry to image Brownian motion within highly scattering media," Opt. Lett. **23**, 319–321 (1998).

63. J. M. Schmitt and S. H. Xiang, "Cross-polarized backscatter in optical coherence tomography of biological tissue," Opt. Lett. **23**, 1060–1062 (1998).

64. J. Broky, K. M. Douglass, J. Ellis, and A. Dogariu, "Fluctuations of scattered waves: going beyond the ensemble average," Opt. Express **17**, 10466–10471 (2009).

65. C. E. Shannon, "A mathematical theory of communication," Bell Syst. Tech. J. **27**, 379–423, 623–656 (1948).

66. I. Freund, "“1001” correlations in random wave fields," Waves in Random Media **8**, 119–158 (1998).

67. A. A. Chabanov, B. Hu, and A. Z. Genack, "Dynamic Correlation in Wave Propagation in Random Media," Phys. Rev. Lett. **93**, 123901 (2004).

68. S. Zhang, B. Hu, P. Sebbah, and A. Z. Genack, "Speckle Evolution of Diffusive and Localized Waves," Phys. Rev. Lett. **99**, 063902 (2007).

69. O. Gilbert, C. Deumié, and C. Amra, "Angle-resolved ellipsometry of scattering patterns from arbitrary surfaces and bulks," Opt. Express **13**, 2403–2418 (2005).

70. J. Sorrentini, M. Zerrad, and C. Amra, "Statistical signatures of random media and their correlation to polarization properties," Opt. Lett. **34**, 2429–2431 (2009).

71. C. Amra, M. Zerrad, L. Siozade, G. Georges, and C. Deumié, "Partial polarization of light induced by random defects at surfaces or bulks," Opt. Express **16**, 10372–10383 (2008).

72. M. Zerrad, J. Sorrentini, G. Soriano, and C. Amra, "Gradual loss of polarization in light scattered from rough surfaces: Electromagnetic prediction," Opt. Express **18**, 15832–15843 (2010).

73. J. Broky, J. Ellis, and A. Dogariu, "Identifying non-stationarities in randomEM fields: are speckles reallydisturbing?," Opt. Express **16**, 14469–14475 (2008).

74. J. Broky and A. Dogariu, "Complex degree of mutual polarization in randomly scattered fields," Opt. Express **18**, 20105–20113 (2010).

75. Y. N. Barabanenkov, Y. A. Kravtsov, V. D. Ozrin, and A. I. Saichev, "II Enhanced Backscattering in Optics," in *Progress in Optics* (Elsevier, 1991), Vol. Volume 29, pp. 65–197.

76. C. Brosseau, *Fundamentals of Polarized Light: a Statistical Optics Approach* (John Wiley, 1998).

77. A. Dogariu, C. Kutsche, P. Likamwa, G. Boreman, and B. Moudgil, "Time-domain depolarization of waves retroreflected from dense colloidal media," Opt. Lett. **22**, 585–587 (1997).

78. L. Tsang and A. Ishimaru, "Backscattering enhancement of random discrete scatterers," J. Opt. Soc. Am. A **1**, 836–839 (1984).

79. M. P. V. Albada and A. Lagendijk, "Observation of Weak Localization of Light in a Random Medium," Phys. Rev. Lett. **55**, 2692–2695 (1985).

80. P.-E. Wolf and G. Maret, "Weak Localization and Coherent Backscattering of Photons in Disordered Media," Phys. Rev. Lett. **55**, 2696–2699 (1985).

81. M. Kaveh, M. Rosenbluh, I. Edrei, and I. Freund, "Weak Localization and Light Scattering from Disordered Solids," Phys. Rev. Lett. **57**, 2049–2052 (1986).

82. E. Akkermans, P. E. Wolf, and R. Maynard, "Coherent Backscattering of Light by Disordered Media: Analysis of the Peak Line Shape," Phys. Rev. Lett. **56**, 1471–1474 (1986).

83. B. P. J. Bret and A. Lagendijk, "Anisotropic enhanced backscattering induced by anisotropic diffusion," Phys. Rev. E **70**, 036601 (2004).

84. D. N. Qu and J. C. Dainty, "Polarization dependence of dynamic light scattering by dense disordered media," Opt. Lett. **13**, 1066–1068 (1988).

85. D. L. Jordan and F. Moreno, "Enhanced backscattering and cross depolarization from multiscale surfaces," J. Opt. Soc. Am. A **10**, 1989–1995 (1993).

86. J. W. Goodman, *Introduction To Fourier Optics* (Roberts and Company Publishers, 2005).

87. S. Huard, *Polarization of Light*, 1st ed. (Wiley, 1997).

88. M. Nieto-Vesperinas and J. A. Sanchez-Gil, "Enhanced long-range correlations of coherent waves reflected from disordered media," Phys. Rev. B **46**, 3112–3115 (1992).

89. L. Tsang and A. Ishimaru, "Theory of backscattering enhancement of random discrete isotropic scatterers based on the summation of all ladder and cyclical terms," J. Opt. Soc. Am. A **2**, 1331–1338 (1985).

90. C. Schwartz and A. Dogariu, "Enhanced backscattering of optical vortex fields," Opt. Lett. **30**, 1431–1433 (2005).

91. I. Freund, "Saddles, singularities, and extrema in random phase fields," Phys. Rev. E **52**, 2348–2360 (1995).

92. I. Freund and D. A. Kessler, "Phase autocorrelation of random wave fields," Optics Communications **124**, 321–332 (1996).

93. M. V. Berry and M. R. Dennis, "Phase singularities in isotropic random waves," Proc. R. Soc. Lond. A **456**, 2059–2079 (2000).

94. M. V. Berry and M. R. Dennis, "Polarization singularities in isotropic random vector waves," Proc. R. Soc. Lond. A **457**, 141–155 (2001).

95. M. S. Soskin, V. Denisenko, and I. Freund, "Optical polarization singularities and elliptic stationary points," Opt. Lett. **28**, 1475–1477 (2003).

96. D. L. Fried, "Laser eye safety: the implications of ordinary speckle statistics and of speckled-speckle statistics," J. Opt. Soc. Am. **71**, 914–916 (1981).

97. B. Ruth, "Superposition of Two Dynamic Speckle Patterns," Journal of Modern Optics **34**, 257–273 (1987).

98. T. Iwai and K. Shigeta, "Experimental Study on the Spatial Correlation Properties of Speckled Speckles Using Digital Speckle Photography," Jpn. J. Appl. Phys. **29**, 1099–1102 (1990).

99. D. Burckel, S. H. Zaidi, A. Frauenglass, M. Lang, and S. R. J. Brueck, "Subfeature speckle interferometry," Opt. Lett. **20**, 315–317 (1995).

100. A. Dogariu and E. Wolf, "Coherence theory of pairs of correlated wave fields," Journal of Modern Optics **50**, 1791–1796 (2003).

101. G. G. Stokes, "Trans. Cambridge Philos Soc. 9 (1852) 399," in *Polarized Light* (Dowden, Hutchinson, and Ross, Inc., 1975).

102. E. Wolf, "Can a light beam be considered to be the sum of a completely polarized and a completely unpolarized beam?," Opt. Lett. **33**, 642–644 (2008).

103. H. Fuji, T. Asakura, and Y. Shindo, "Measurement of surface roughness properties by means of laser speckle techniques," Optics Communications **16**, 68–72 (1976).

104. J. Broky and A. Dogariu, "Correlations of polarization in random electro-magnetic fields," Opt. Express **19**, 15711–15719 (2011).

105. M. Giglio, M. Carpineti, and A. Vailati, "Space Intensity Correlations in the Near Field of the Scattered Light: A Direct Measurement of the Density Correlation Function g(r)," Phys. Rev. Lett. **85**, 1416–1419 (2000).

106. M. Giglio, M. Carpineti, A. Vailati, and D. Brogioli, "Near-Field Intensity Correlations of Scattered Light," Appl. Opt. **40**, 4036–4040 (2001).

107. J. Broky and A. Dogariu, "Polarization correlations in backscattering from media with different optical densities," (In Preparation).

108. P. Sheng, *Scattering and Localization of Classical Waves in Random Media* (World Scientific, 1990).

109. S. Etemad, R. Thompson, and M. J. Andrejco, "Weak Localization of Photons: Universal Fluctuations and Ensemble Averaging," Phys. Rev. Lett. **57**, 575–578 (1986).